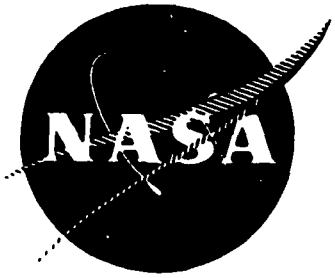

NASA CR - 121038

EXPERIMENTAL INVESTIGATION OF A THROTTLABLE 15 CM HOLLOW CATHODE ION THRUSTER

PREPARED FOR
LEWIS RESEARCH CENTER
NATIONAL AERONAUTICS AND SPACE ADMINISTRATION

GRANT NGR-06-002-112

Annual Report

December 1972

Department of Mechanical Engineering
Colorado State University
Fort Collins, Colorado

1. Report No.	2. Government Accession No.	3. Recipient's Catalog No.
NASA CR-121038		

4. Title and Subtitle	5. Report Date
Experimental Investigation of a Throttlable 15 cm Hollow Cathode Ion Thruster	December 1972
	6. Performing Organization Code
7. Author(s)	8. Performing Organization Report No.
Paul J. Wilbur	
	10. Work Unit No.
9. Performing Organization Name and Address	11. Contract or Grant No.
Department of Mechanical Engineering Colorado State University Fort Collins, Colorado 80521	NGR-06-002-112
	13. Type of Report and Period Covered Contractor Report Dec. 1, 1971 - Dec. 1, 1972
12. Sponsoring Agency Name and Address	14. Sponsoring Agency Code
National Aeronautics and Space Administration Washington, D. C. 20546	

15. Supplementary Notes

Grant Monitor, William Kerslake
Spacecraft Technology Div.
NASA Lewis Research Center
Cleveland, Ohio 44135

16. Abstract

The use of dished high perveance grids on a 15 cm modified SERT II thruster is shown to facilitate throttled operation over a beam current range from 60 to 600 ma. Effects of increasing the radial component of the magnetic field in the main discharge chamber and decreasing the dimensions of the cathode discharge region are examined and found to degrade performance to the extent that primary electrons are forced in toward the center-line of the thruster. Studies of the baffle aperture region of two thrusters indicate that the electric potential gradient vector is perpendicular to the local magnetic field lines when the thruster is operating properly. The correlation between the shape of the ion beam current density and that of the ion density at the screen grid within the thruster is shown to be 94%. Additional experimental studies on maximum propellant utilization, plasma ion production cost, neutral density in the cathode discharge region, double ion production in hollow cathode thrusters and thermal flow meter performance are discussed.

17. Key Words (Suggested by Author(s))	18. Distribution Statement
Electrostatic Thruster	Unclassified - Unlimited

19. Security Classif. (of this report)	20. Security Classif. (of this page)	21. No. of Pages	22. Price*
Unclassified	Unclassified	69	$3.00

*For sale by the Clearinghouse for Federal Scientific and Technical Information
Springfield, Virginia 22151

NASA-C-168 (Rev. 7-70)

TABLE OF CONTENTS

LIST OF FIGURES

LIST OF TABLES

INTRODUCTION

The research described in this report is centered around the evolution of a 15 cm thruster which can be operated at a beam current through the range 375 ma to 75 ma with an ion beam profile that is as flat as possible and reasonable propellant utilization and power efficiencies. Emphasis has also been placed on understanding thruster phenomena observed as modifications are made to the thruster, and this has necessitated extensive Langmuir probing of the main and cathode discharge regions of the thruster to determine plasma property contours. Because of the large amount of data involved only a fraction of these contours are included in the report. The complete set is available from the author upon request.

Research into the effects of the hollow cathode discharge on throttled performance of a 20 cm thruster was completed during the period covered by this report. This work was reported in reference 1 and is not reproduced here.

APPARATUS AND PROCEDURE

The bulk of the mercury electron bombardment ion thruster research described herein was conducted on a 15 cm dia SERT II thruster[2,3] which had been modified to permit: (1) independent control and measurement of mercury flow rates to the neutralizer, hollow cathode and main propellant flow distributor and (2) variation of magnetic field intensity. Mercury flow rates were determined by timing the fall of a column of mercury in 0.9 mm bore glass tubes in accordance with the procedures discussed in reference (4). Cathode and main propellant flows were separated by plugging the SERT II flow dividing orifice located downstream of the mock isolator and installing a second vaporizer which supplied flow directly into the main flow distribution chamber which had been fed by this orifice. Magnetic field intensity control was achieved by removing the eight SERT II permanent magnets and installing electromagnets in their place. Gaussmeter measurements were used to determine that an electromagnet current of 7.0a produced about the same magnetic field intensities as the permanent magnets in the standard thruster configuration.

Electrical power was supplied to the thruster by a series of power supplies arranged in the manner shown in Figure 1. Arc voltage, arc current, keeper voltage and ion beam current were displayed on digital voltmeters as suggested by this schematic.

Langmuir probes which could be swept through a semicircular arc and moved axially during thruster operation were installed in both the main and cathode discharge regions in the manner suggested by Figure 2. The Langmuir probe output recording system and the Faraday probe system used to determine ion beam current density profiles are described in reference (4).

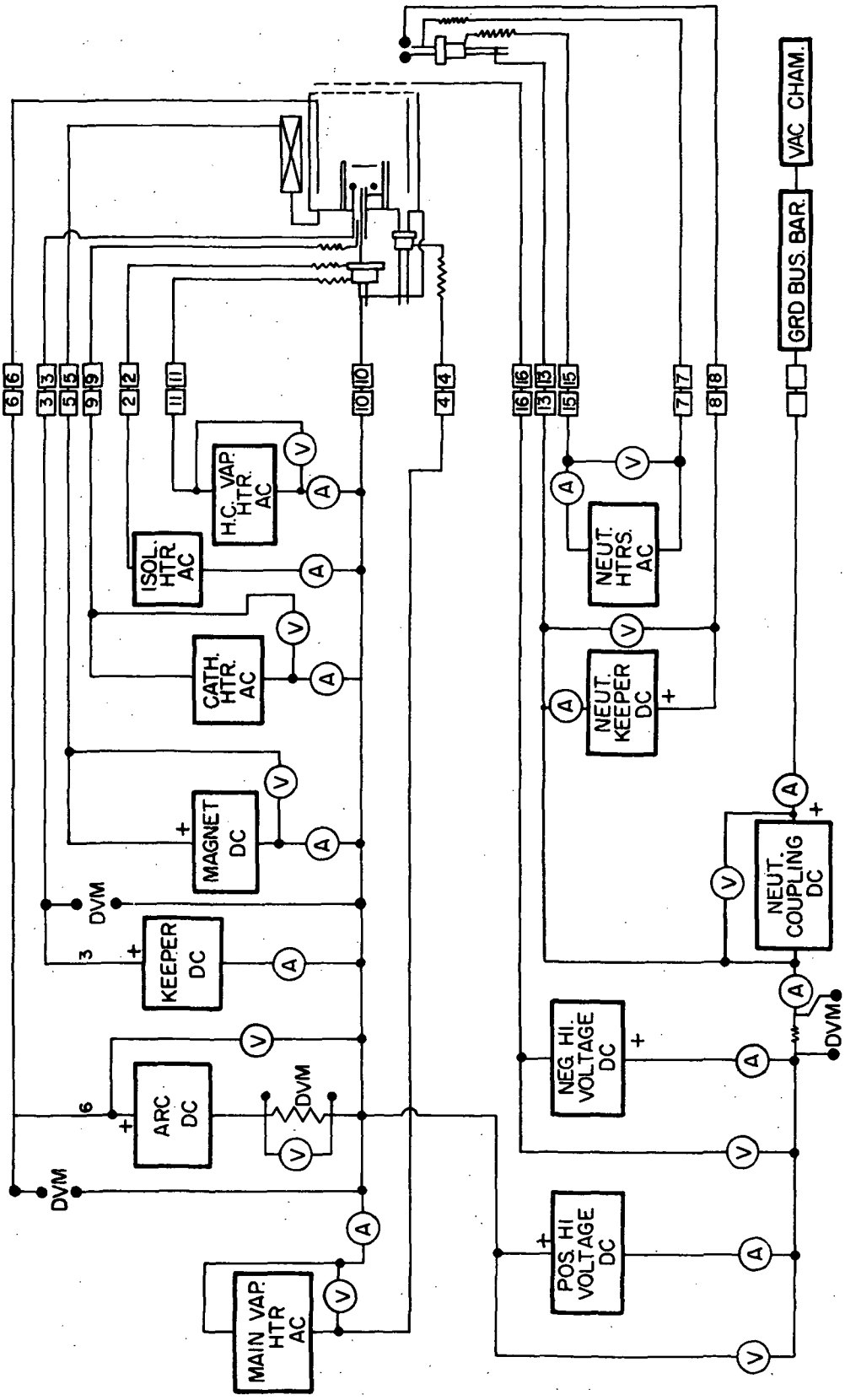

FIGURE 1. POWER SYSTEM SCHEMATIC

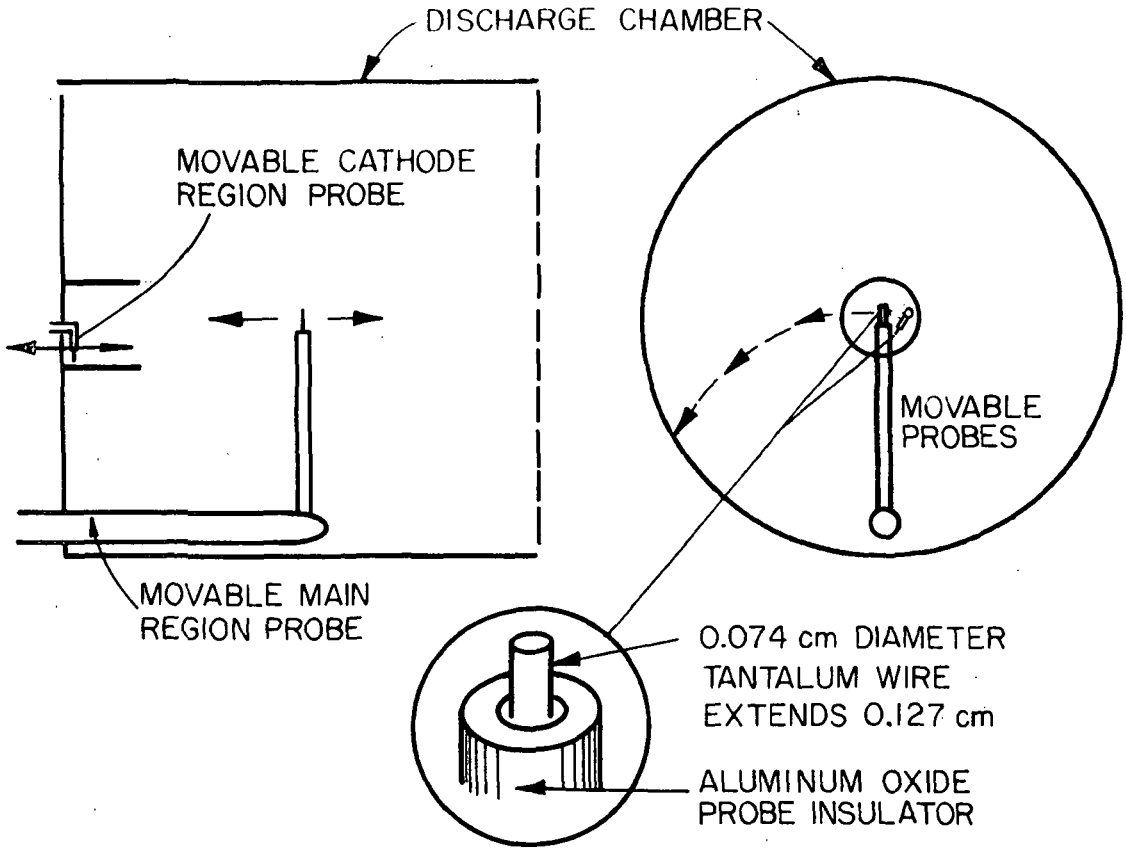

FIGURE 2. LANGMUIR PROBES

In order to verify the standard 100% thrust level operating conditions, the modified thruster was operated at the currents and voltage levels reported in reference (5). A comparison between previously reported data and those obtained in this test is presented as Table I. With the exception of the beam current which was 18 ma low in the C.S.U. test, the correspondence was very close. This discrepancy was considered to be due to a slightly different flow distribution between the main and cathode flow sources.

After the performance verification described above, the six holes in the SERT II baffle were closed off and the grid potentials were changed from + 3 kv and - 1.5 kv to ± 1.6 kv. The lower screen grid potential (+ 1.6 kv) was selected to give a lower specific impulse (3400 sec @ 85% utilization) than that of SERT II. The accelerator grid potential (- 1.6 kv) was used in spite of an expected defocussing of the ion beam in an effort to achieve a high beam current (at least 375 ma). Subsequent tests showed a 375 ma beam could be achieved with these potentials only under penalty of excessive discharge losses. As a result the grid potentials were changed to + 3.4 kv, - 1.7 kv where the 375 ma beam could be drawn at a reasonable discharge loss level. It was argued that substitution of higher perveance grids at some later time would permit operation at the same beam current/discharge loss condition at lower grid potentials.

15 cm thruster data presented in this report were obtained at + 3.4 kv, - 1.7 kv grid potentials unless otherwise identified. Tests reported herein were performed with a 0.3a keeper current and with a hollow cathode having a 0.05 cm dia orifice. This orifice which is larger than that used on SERT II was used because future operations at high beam and hence

Table I
SERT II Performance Comparison
at 100% Thrust Level

	NASA Lewis Tests[5]	CSU Test
Cathode Vaporizer heater current	1.7 to 1.9a	1.8a (a.c.)
Main Vaporizer heater current	1.7 to 1.9a	1.7a (a.c.)
Thruster Cathode heater current	1.5a**	7.1a (a.c.)
Discharge voltage	36.9 to 37.3v	37v
Discharge current	1.8a to 1.57a	1.7a
Positive high voltage	3 kv	3 kv
Screen current	253 ma	235 ma
Negative high voltage	- 1.5 kv	- 1.5 kv
Accelerator current	1.6 to 1.3 ma	1.4 ma
Neut. vaporizer and cathode heater current	1.8 to 2.1a	2.1a (a.c.)
Neut. keeper voltage	23 v	27 v
Neut. keeper current	0.182a to 0.2a	0.2a
Neut. cathode to tank wall voltage	-14v to -17.5v	-14.5v
Neut. emission current	~250 ma	235 ma
Thruster cathode keeper voltage	12.3v to 10.7v	10.7v
Thruster cathode keeper current	0.3a	0.3a
Pressure of thruster environment	4 to 5x10-6 torr	3x10-6 torr
Main flow rate	*	206 ma eq
Cathode flow rate	*	107 ma eq
Neut. flow rate	17 ma eq	18 ma eq
Magnet current	***	7a

* SERT II contained a single vaporizer and an orifice which split the flow, so flows were not measured (total flow ~ 313 ma)

** The SERT II flame sprayed cathode heater was replaced by a metal encapsulated heater wound around the cathode tip. The power output of this heater at 7.1a current is about twice that of the SERT II heater at its nominal operating current (1.5a).

*** SERT II had permanent magnets.

arc current conditions were anticipated. The larger orifice did not affect plasma conditions in the cathode discharge region noticeably.

Because the thruster was to be throttled to low beam current conditions where keeper power consumption could be significant beam ion costs (ev/ion) include keeper power throughout the report.

15 CM THRUSTER PERFORMANCE STUDIES

The objective of this work was the evolution of a 15 cm thruster that could be throttled over a five-to-one range while holding discharge losses near 200 ev/ion and operating at a specific impulse below that of SERT II (~Vnet = 3 kv). An additional objective was the flattening of the ion beam current density profile.

Moveable Cathode Pole Piece

In view of the success achieved by Knauer et. al.[6] in flattening the ion beam profile and reducing arc discharge losses in the radial field thruster, the initial attempt at improving the thruster centered on increasing the radial component of the magnetic field in the main discharge chamber. In order to vary this component, the cathode pole piece was modified so its length could be adjusted during thruster operation. This was accomplished by installing a moveable iron sleeve within the SERT II cathode pole piece. When the sleeve was moved, the cathode and baffle moved with it so the cathode discharge region configuration was unaltered. Magnetic field maps obtained with the sleeve flush with the pole piece, extended 3 cm and extended 5.5 cm are presented as Figures 3, 4, and 5 respectively. The increase in the radial component of the magnetic field which can be achieved is particularly apparent when Figures 3 and 5 are compared.

The effect of extending the cathode pole piece on thruster performance is shown in Figure 6 for a total flow ($\dot{m}_T$) of 440 ma eq. The solid symbols indicate the 37 v arc voltage condition.

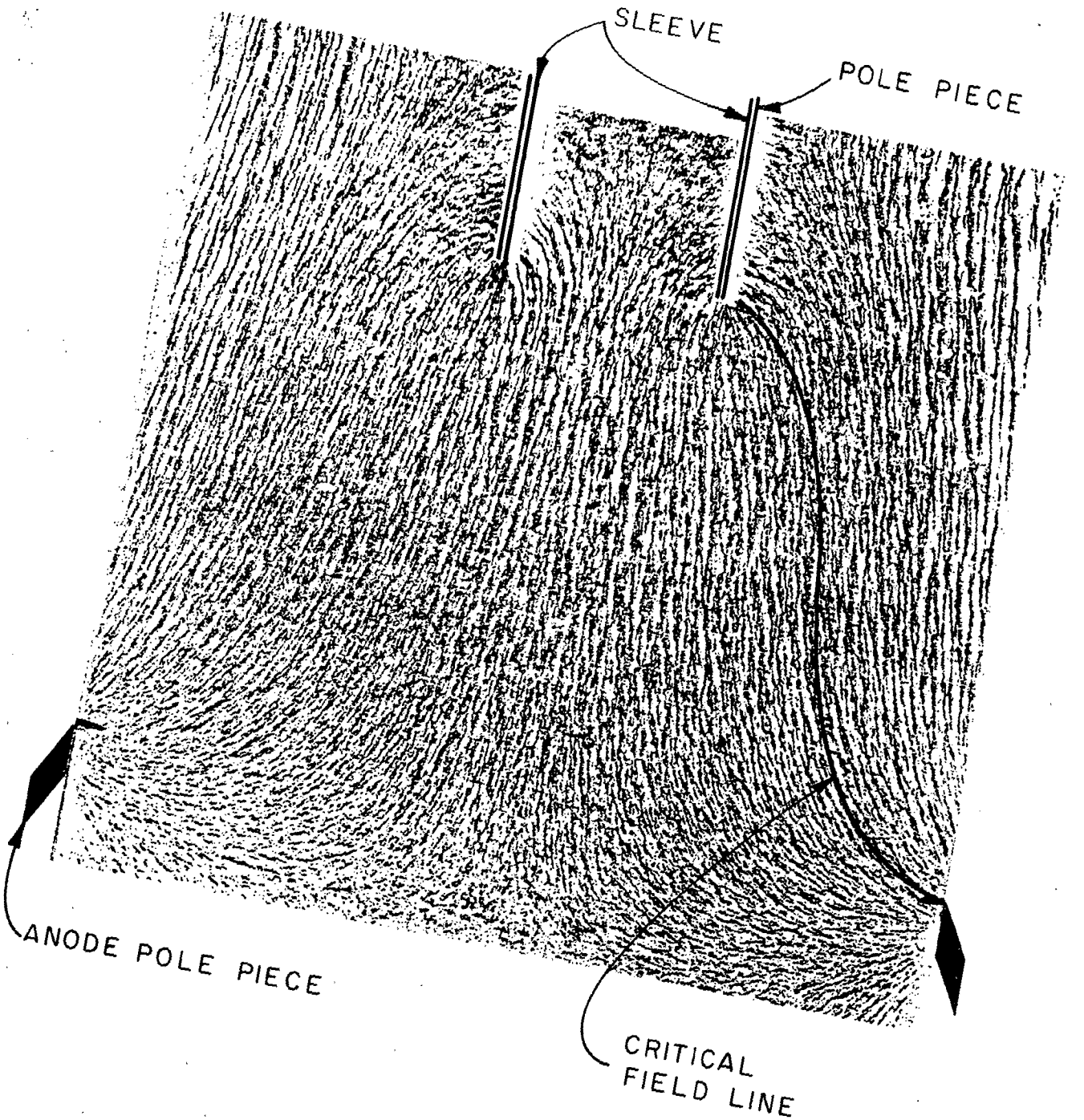

FIGURE 3. MAGNETIC FIELD MAP
(SLEEVE FLUSH)

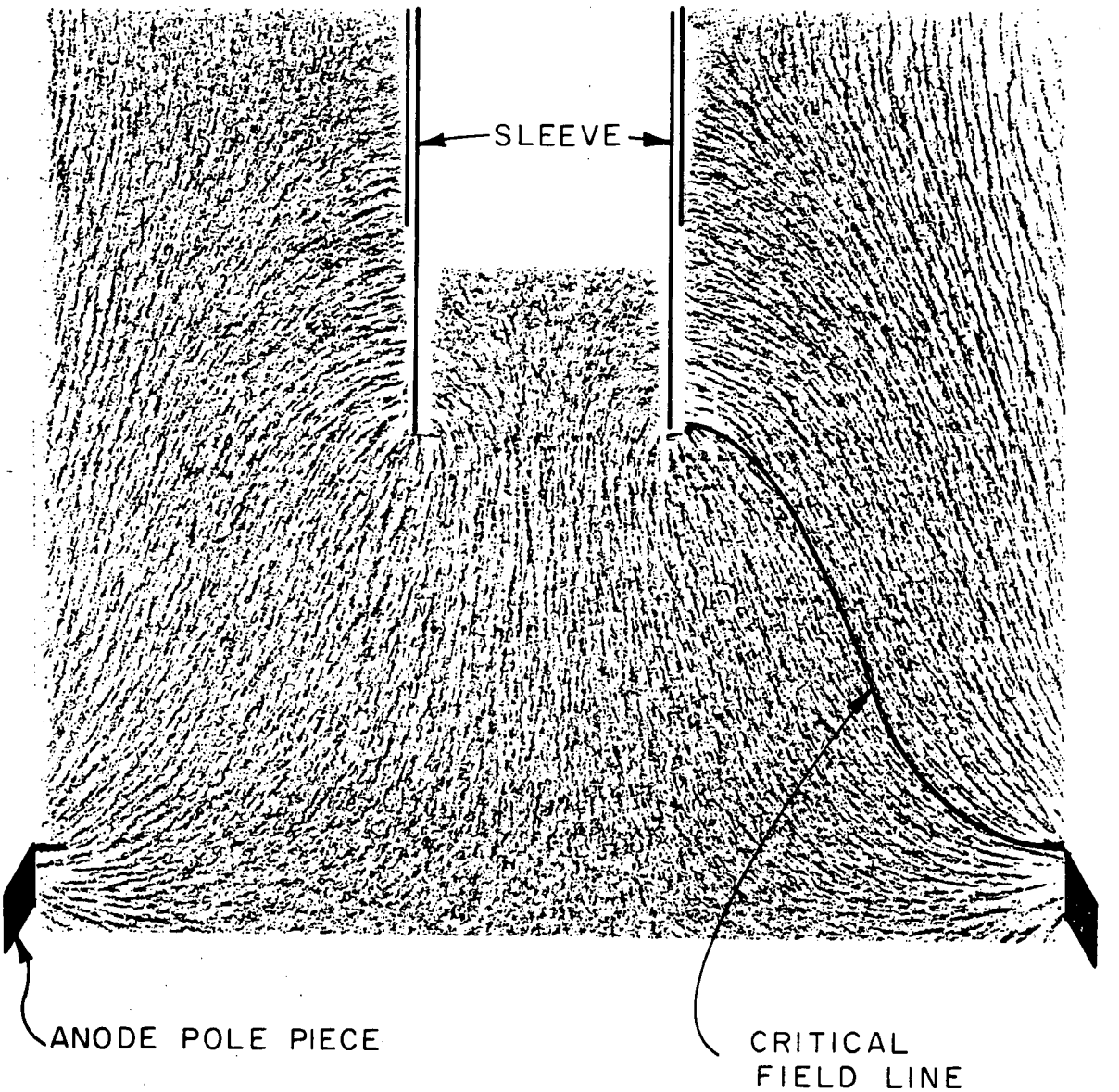

FIGURE 4. MAGNETIC FIELD MAP
(SLEEVE EXTENDED 3 CM)

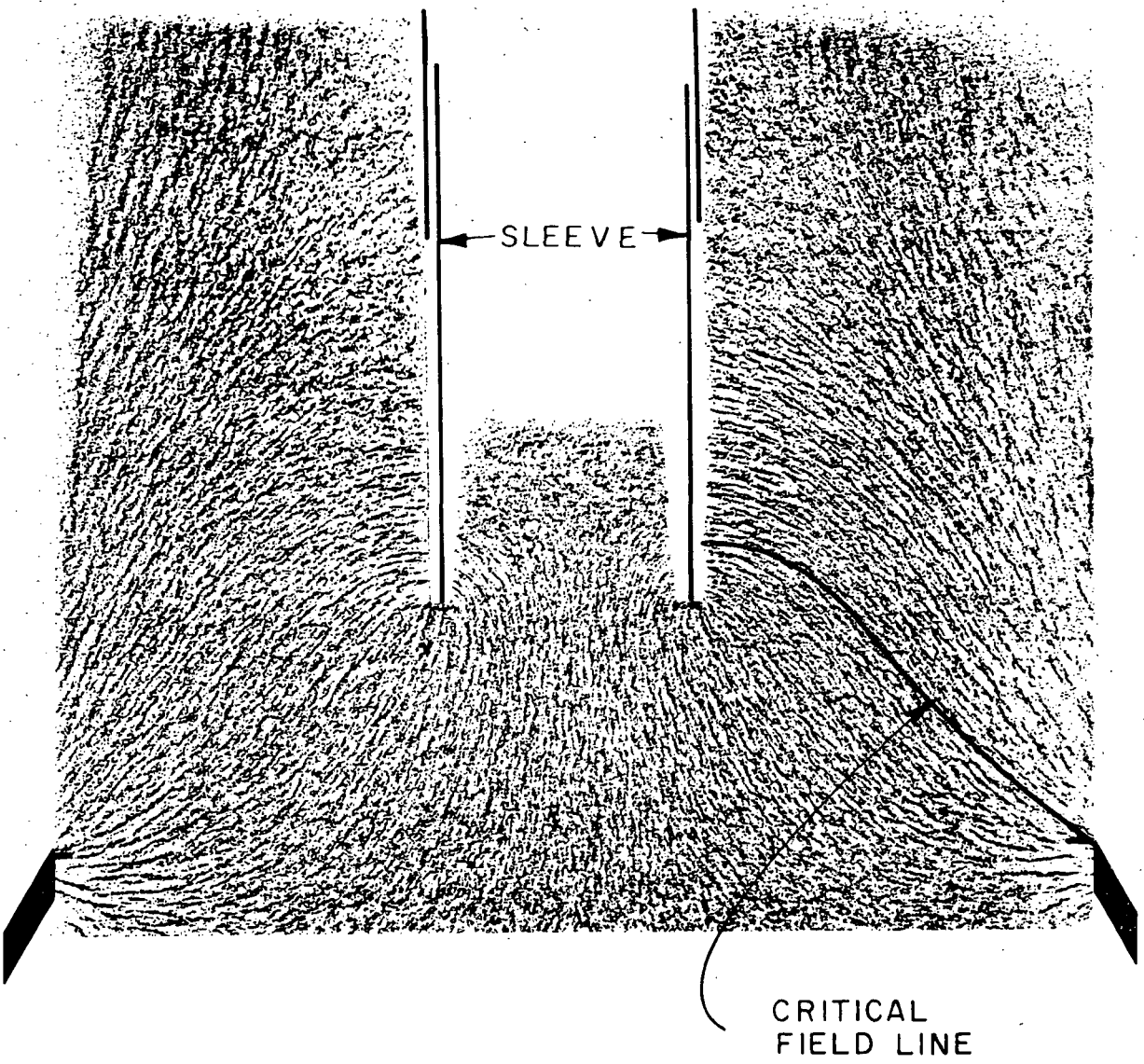

FIGURE 5. MAGNETIC FIELD MAP
(SLEEVE EXTENDED 5.5 CM)

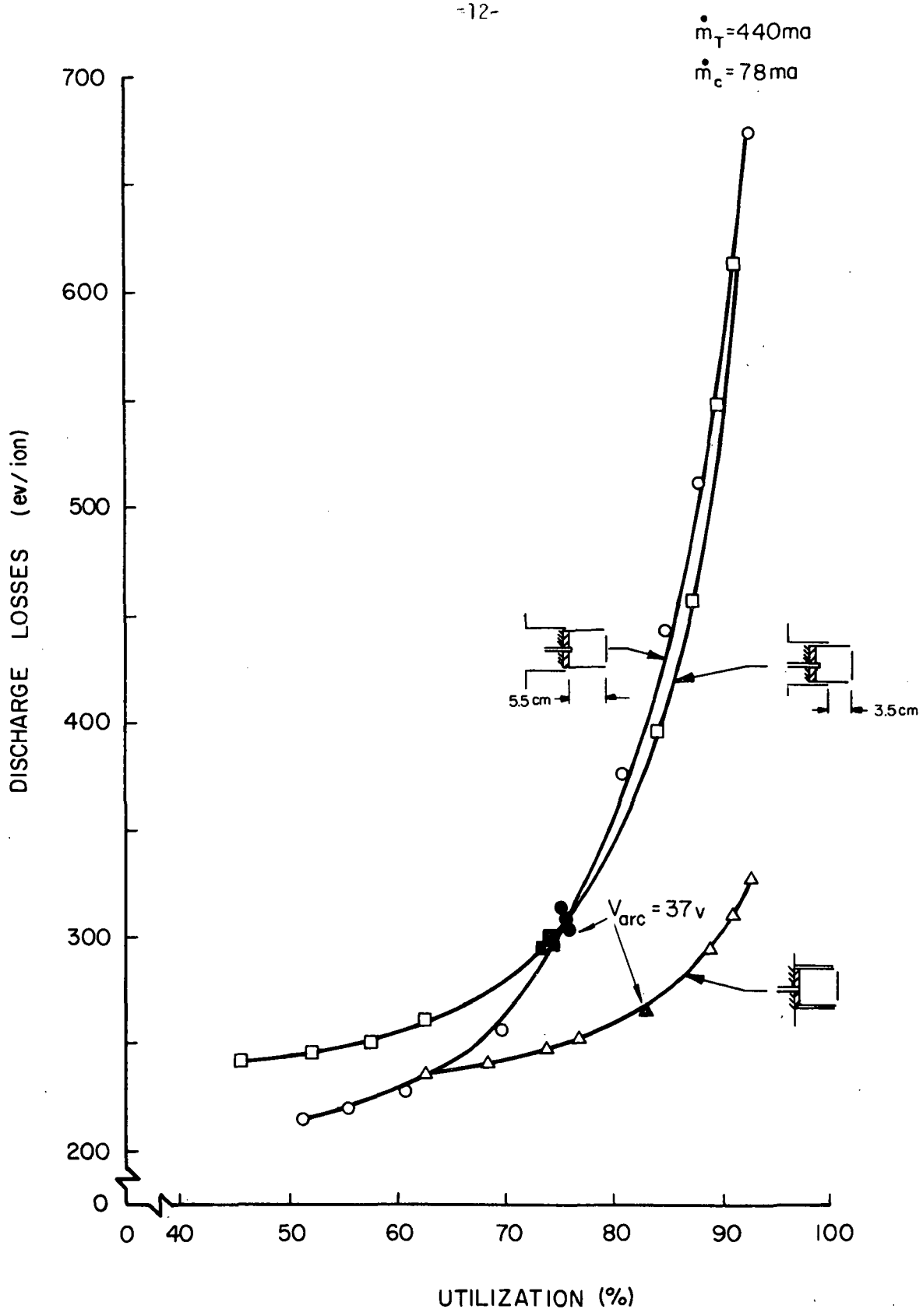

FIGURE 6. EFFECT OF POLE PIECE LENGTH ON PERFORMANCE

m_c indicates the flow rate through the hollow cathode. These data indicate thruster performance is degraded by operation with the cathode pole piece extended. Figure 7 presents similar data obtained at a 220 ma total flow rate. These data again indicate performance is degraded by an extension of the cathode pole piece. The arc voltage range over which the 220 ma flow rate data were gathered with the sleeve extended was centered around 29 v as indicated on Figure 7 rather than the more typical 37 v. The higher base line discharge losses observed with the extended pole piece in Figure 7 are attributed to this lower arc voltage operation.

The low arc voltage conditions shown on Figure 7 were caused by high cathode flow rates which were employed when the cathode pole piece was extended because they tended to give the best performance. This effect is shown in Figure 8. At a given flow performance was also optimum at specific keeper and magnet currents; these optimum values for the flows of Figure 8 are indicated. Although arc voltage could be increased by reducing the cathode flow rate, this increase in arc voltage was not accompanied by improved performance. The reason for this can be understood if one considers the primary electron density plots of Figure 9. Figure 9a corresponds to the case where the cathode pole piece length is the standard SERT II length and Figure 9b to the case where it has been extended 3 cm. A comparison shows the primary electrons are concentrated near the thruster axis and toward the screen grid when the pole piece is extended. Since neutral atoms are most likely to be ionized if they are introduced into a high primary electron density region, lower discharge loss operation is congruent with neutral atom introduction through the hollow cathode. In retrospect this could have been predicted by consideration of the magnetic field maps (Figures 3 to 5) which indicate the region of primary electron containment within critical

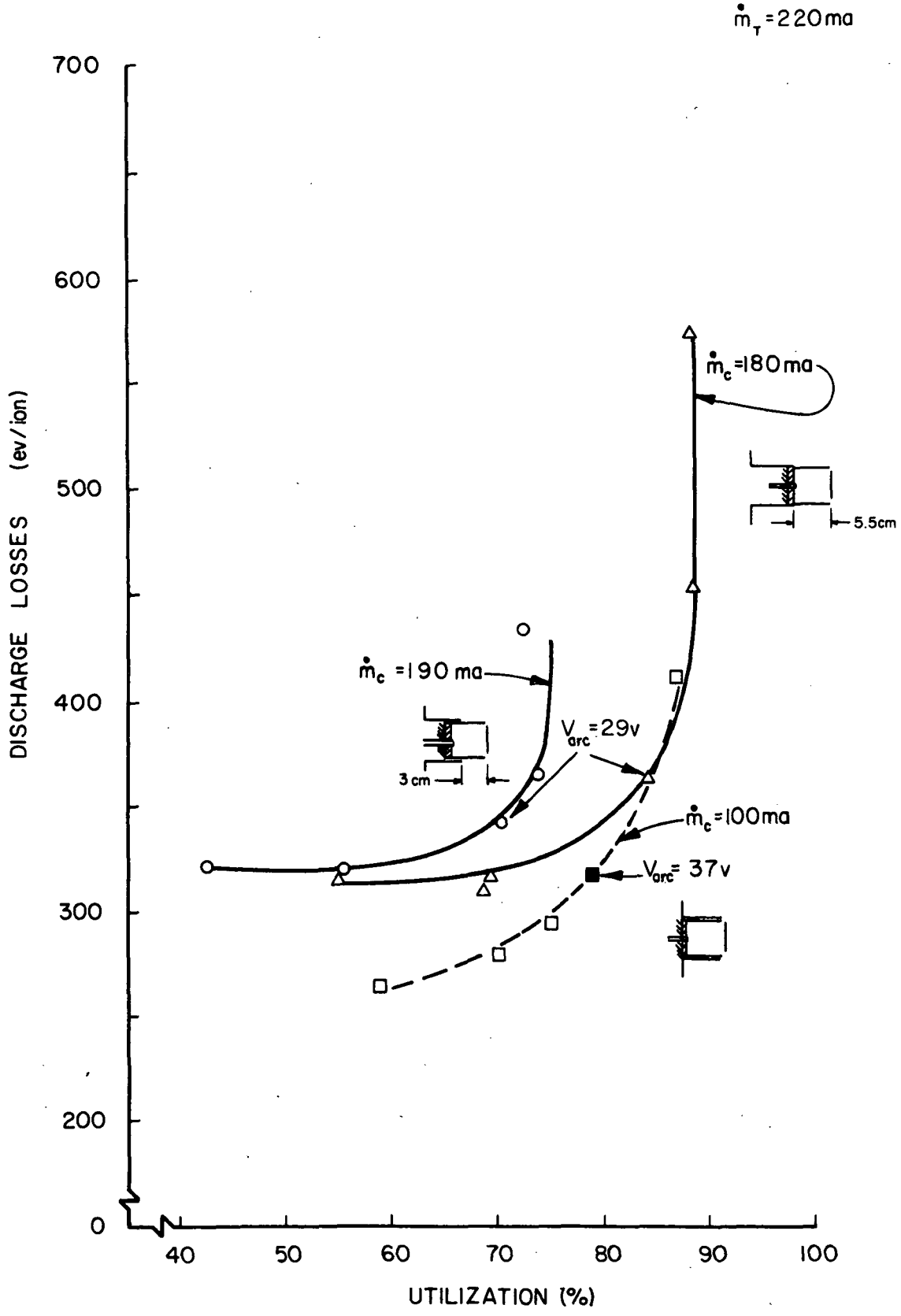

FIGURE 7. EFFECT OF POLE PIECE LENGTH ON PERFORMANCE

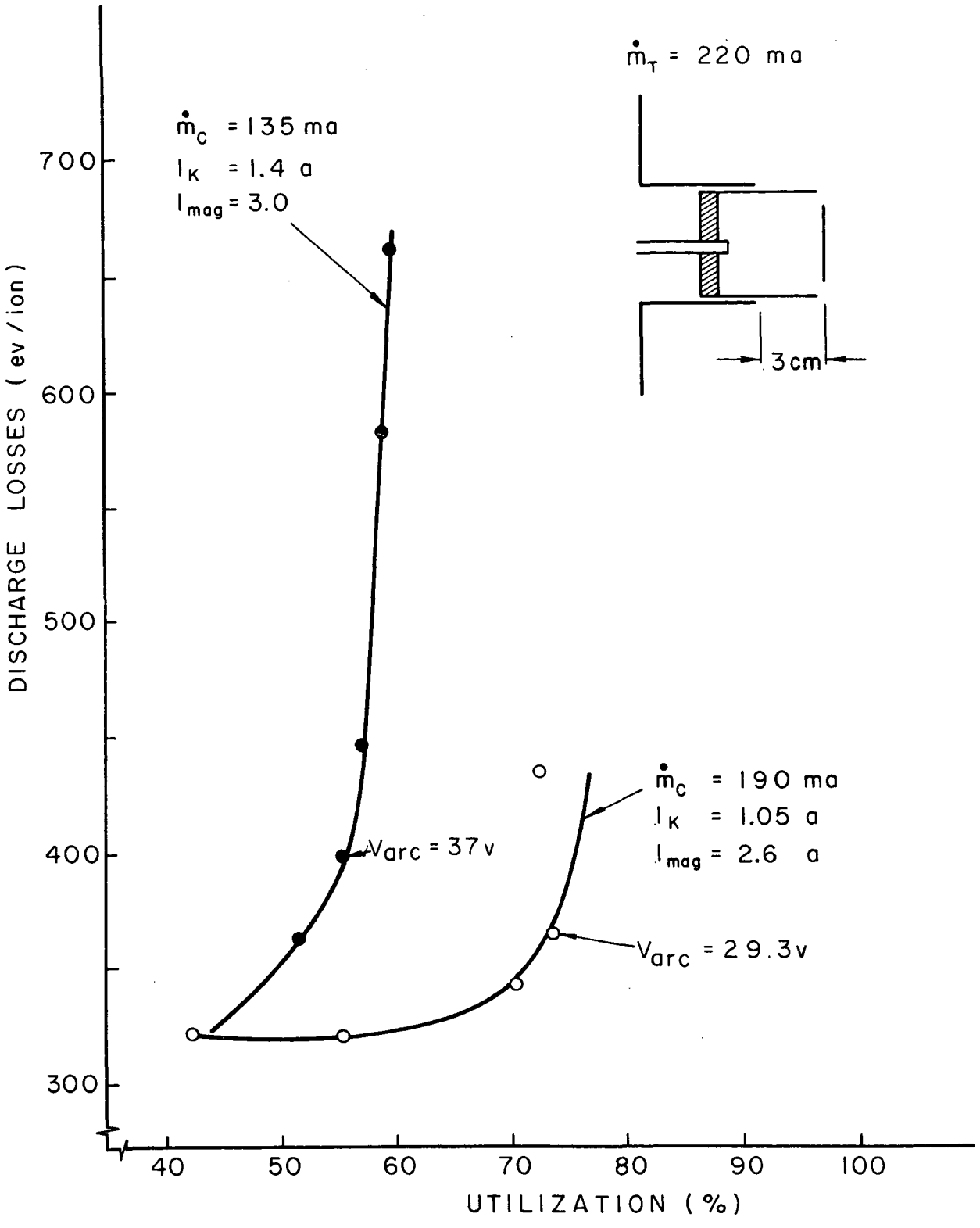

FIGURE 8. EFFECT OF CATHODE FLOW RATE ON PERFORMANCE

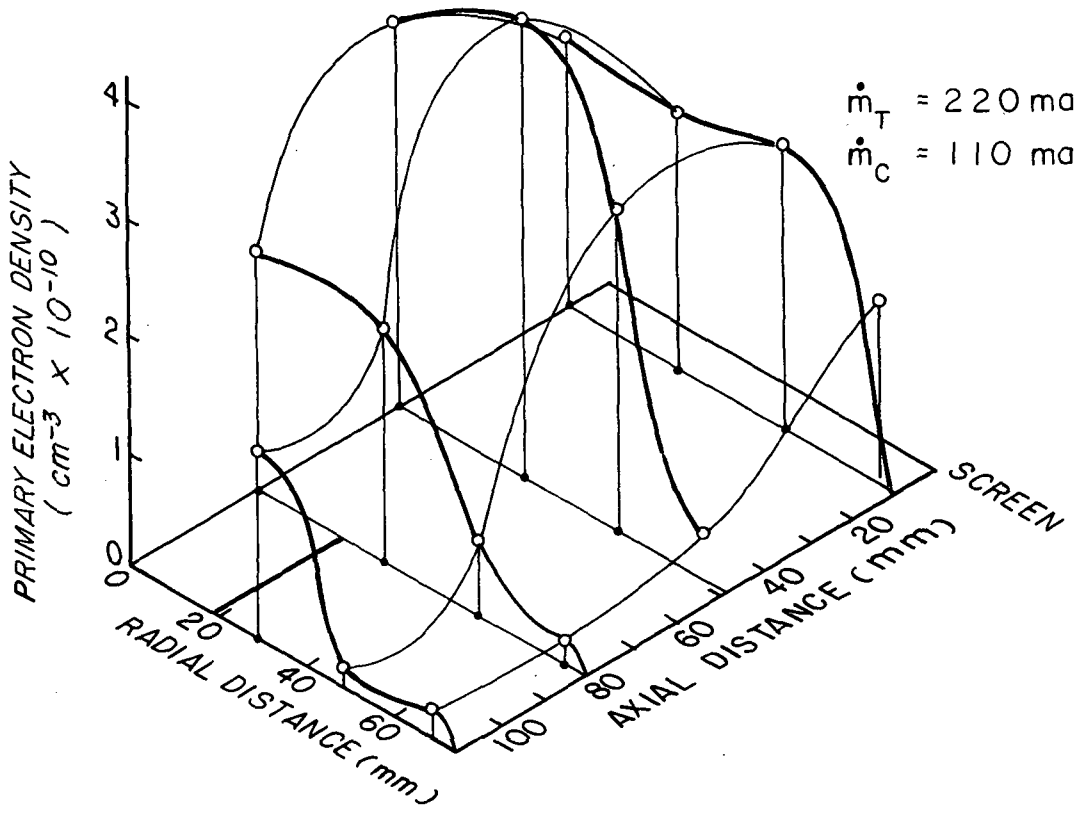

(a) POLE PIECE SLEEVE FLUSH

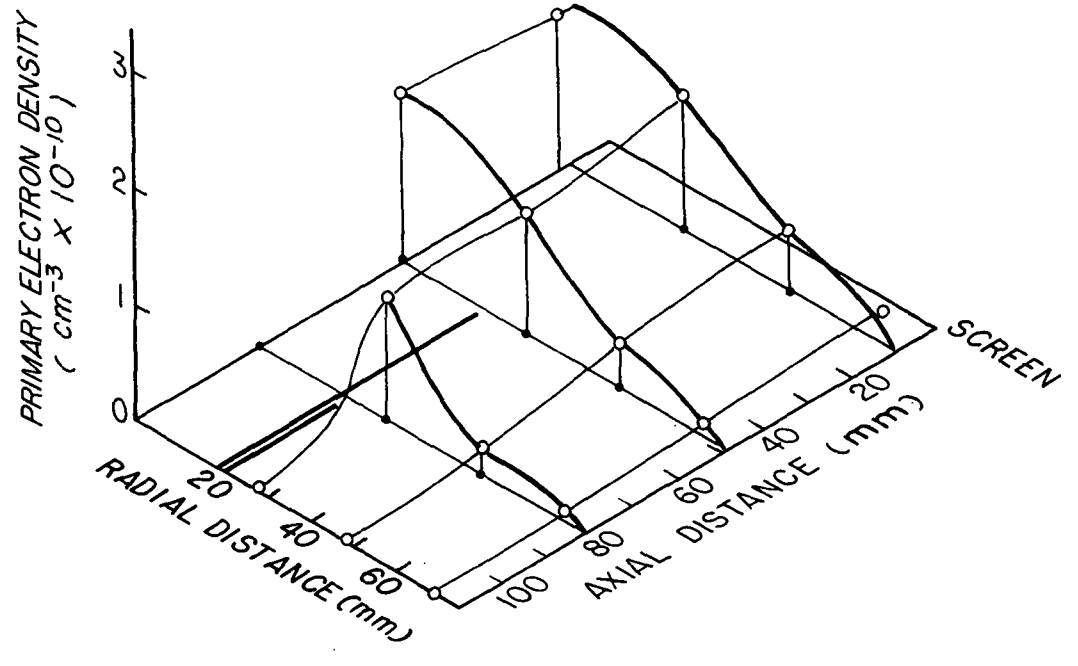

(b) POLE PIECE EXTENDED 3 cm

FIGURE 9. PRIMARY ELECTRON DENSITY CONTOURS

field lines[7]. These lines are seen to confine the primary electrons near the centerline of the discharge chamber as the pole piece is extended.

Figure 10 shows the primary electron density contours at a 440 ma total flow rate for the cases of pole piece sleeve flush and extended. The effect of extending the sleeve is the same as it was at the low flow rate.

Results of this study showed a universal degradation in performance accompanied any extension of the cathode pole piece beyond the SERT II design and therefore this method of improving thruster performance was abandoned. Again in retrospect this conclusion was predictable based on 1) the magnetic field maps (Figures 3 to 5) which indicate the region of primary electron density and 2) the Kaufman model for maximum propellant utilization[8] which shows highest propellant utilization is achieved when the volume to surface area ratio of the primary electron region is a maximum (larger primary electron regions).

Decreased Cathode Discharge Region Dimensions

Because some success had been achieved in improving the throttled performance of a 20 cm thruster through reductions in the cathode discharge region dimensions[4], this was attempted next on the 15 cm thruster. The effect of reducing the standard SERT II cathode pole piece diameter and length to obtain a 2 cm dia by 1.7 cm long cathode discharge region are indicated in Figures 11, 12, and 13 for 440 ma, 220 ma and lesser total flows respectively. The baffle diameter was 2.34 cm which was the same as the outside diameter of the end of the pole piece. Figure 11 indicates the smaller pole piece causes a reduction in the maximum

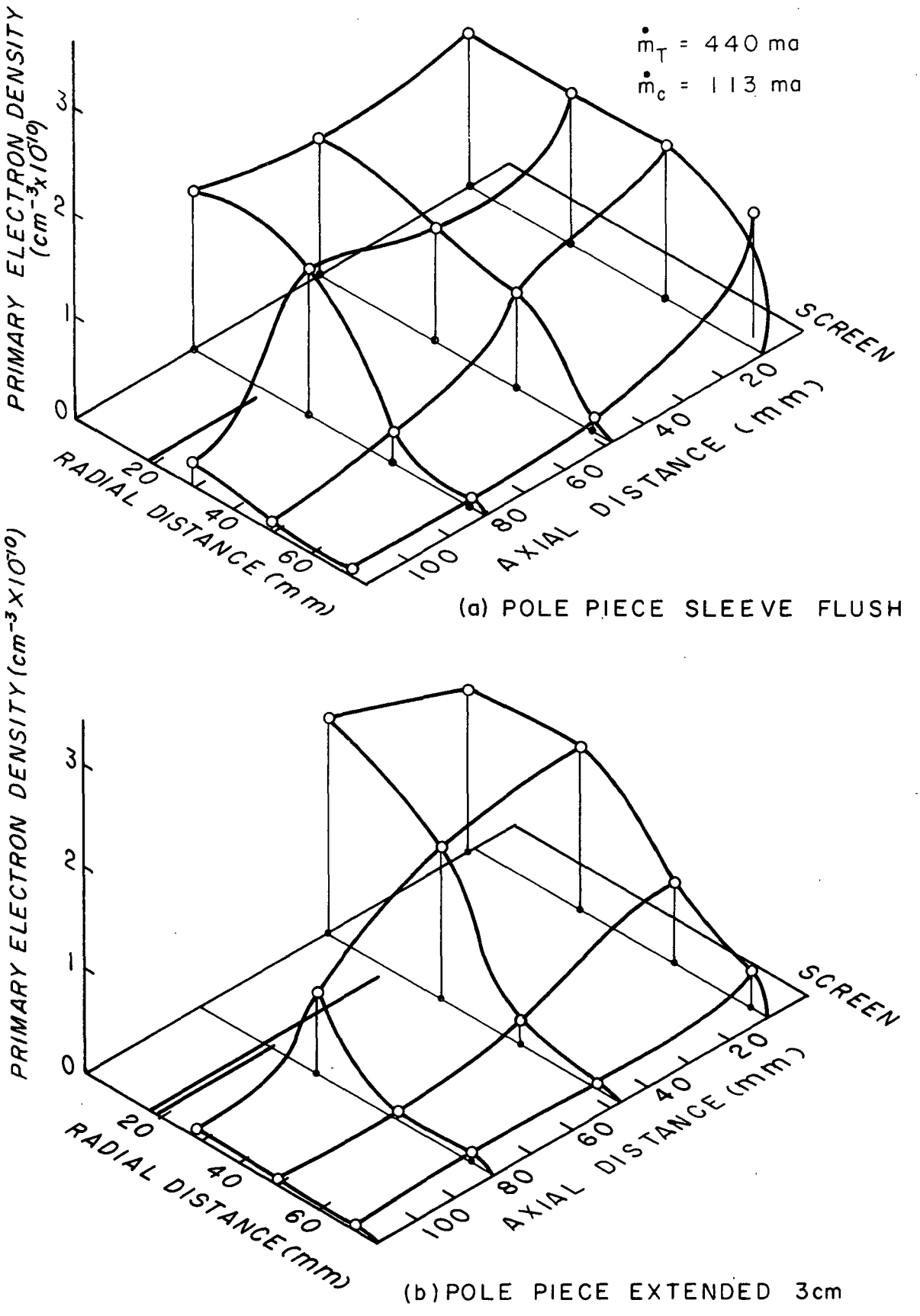

FIGURE 10. PRIMARY ELECTRON DENSITY CONTOURS

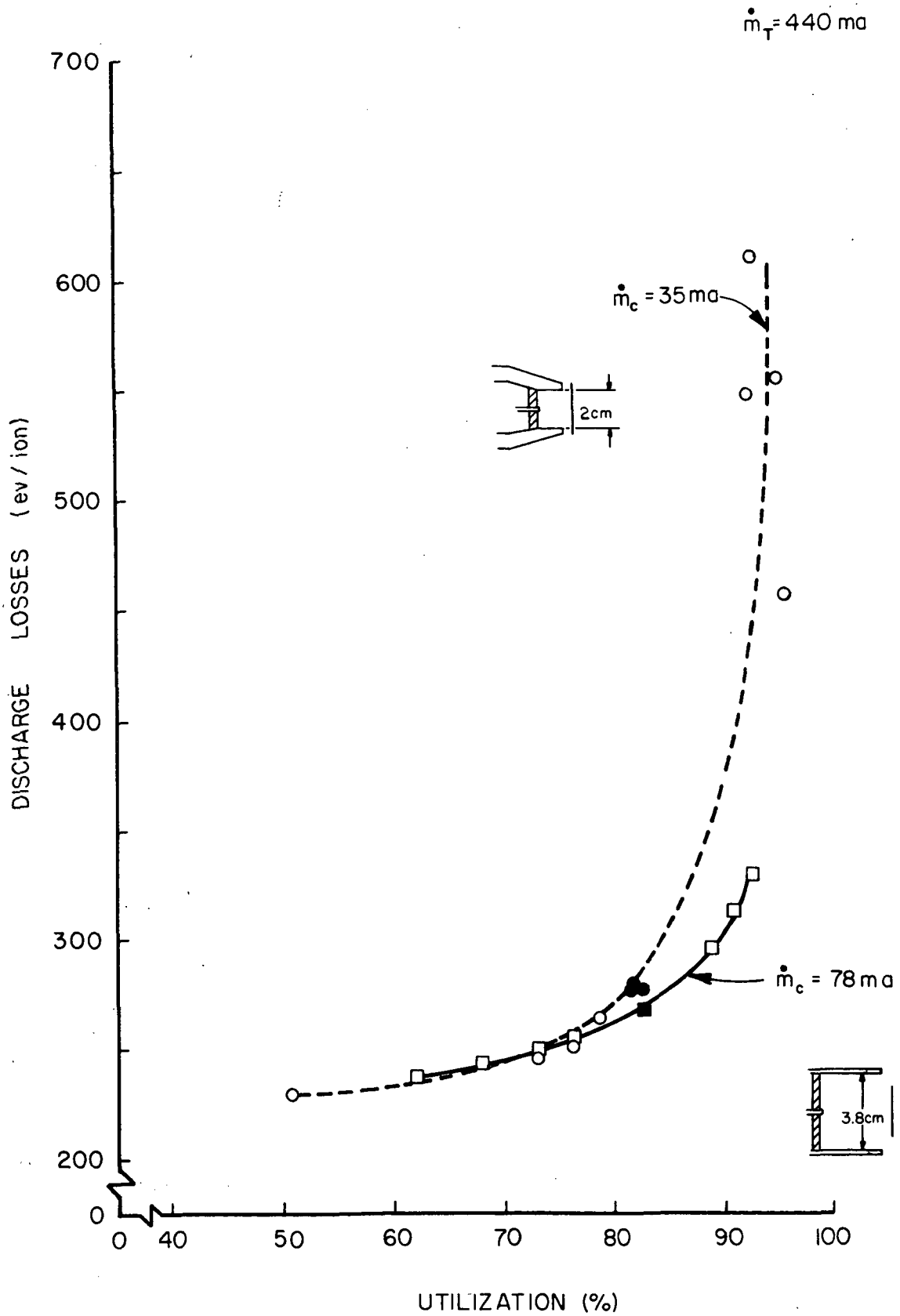

FIGURE 11. EFFECT OF CATHODE POLE PIECE DIAMETER

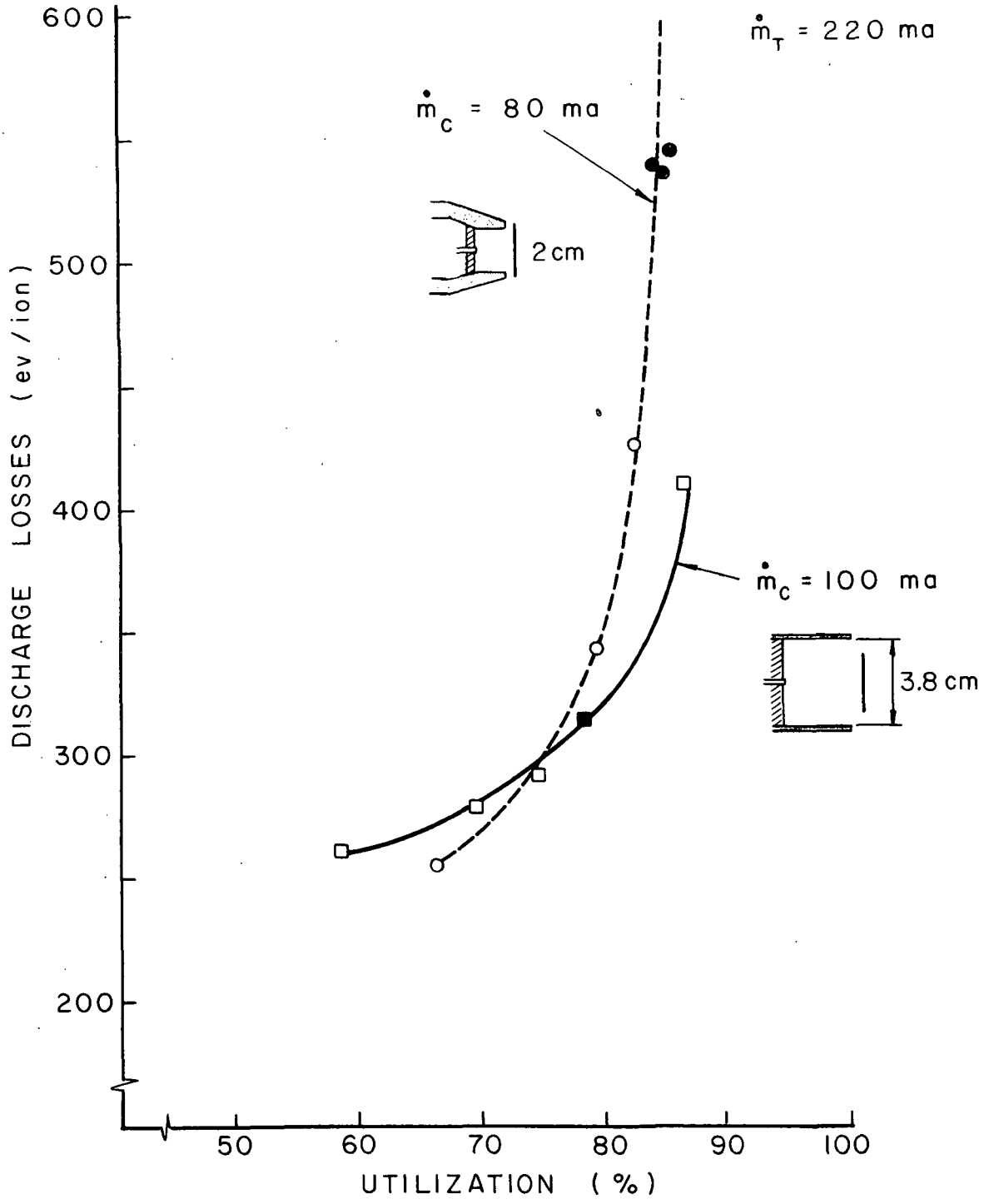

FIGURE 12. EFFECT OF CATHODE POLE PIECE DIAMETER

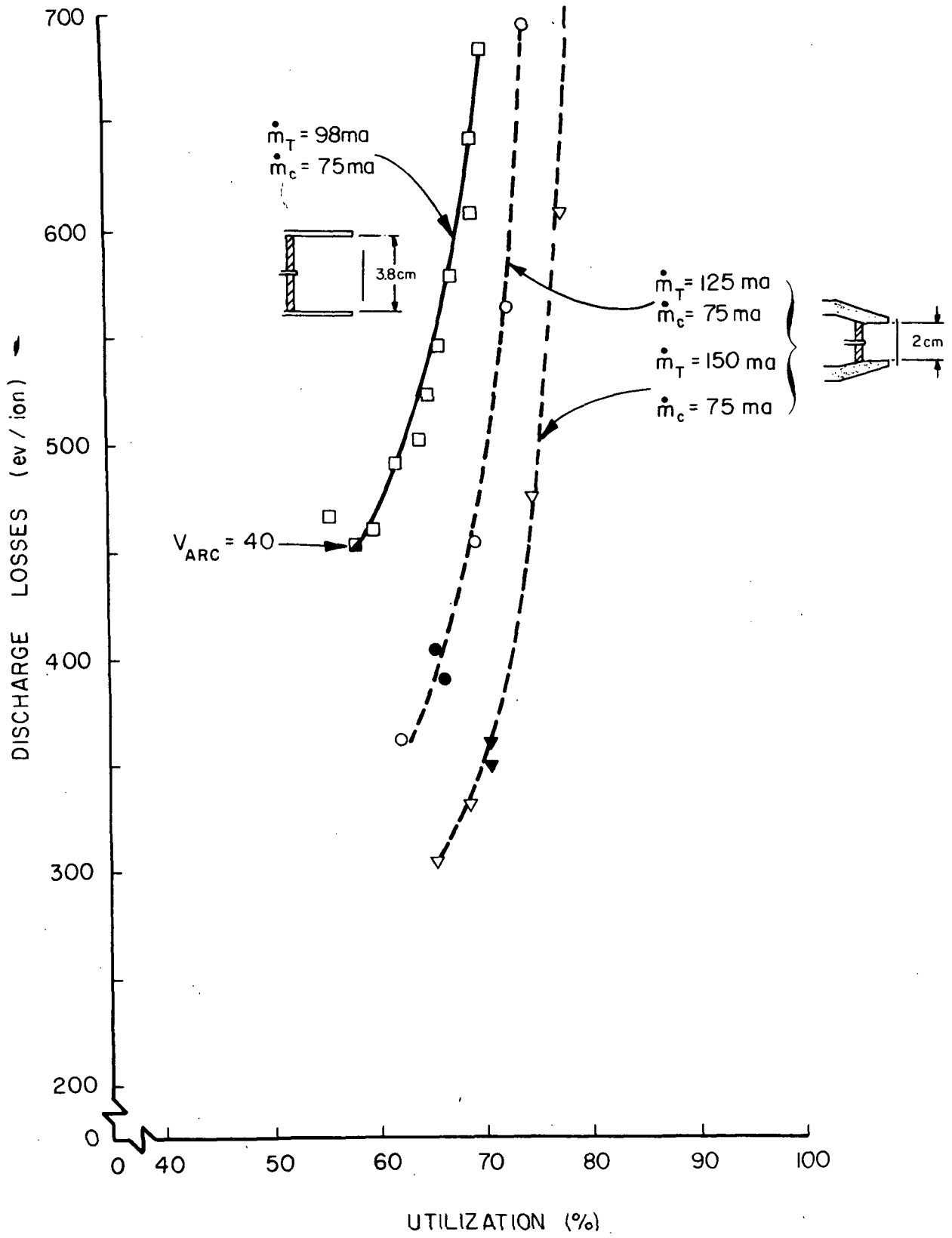

FIGURE 13. EFFECT OF CATHODE POLE PIECE DIAMETER

utilization and no change in the base line discharge losses. Figure 12 for a 220 ma total flow also shows the 2 cm dia pole piece reduces the maximum utilization efficiency, but it suggests lower base line discharge losses are obtained. Figure 13 suggests lower base line discharge losses will be obtained and that operation can be sustained readily at voltages below 40 v when the 2 cm dia pole piece is substituted and total flow is below 220 ma. Figures 11 and 12 also indicate lower cathode flow rates are required when the 2 cm dia cathode pole piece is substituted for the standard SERT II unit. Figure 13 indicates the cathode flow requirement is not changed significantly at very low total flows with substitution of the smaller pole piece. In general stable thruster operation was found over greater arc voltage and flow ranges when the small cathode discharge region was employed.

The reason for the reduction in maximum utilization observed for total flows of 440 ma and 220 ma with the 2 cm dia pole piece can be seen in Figure 14, the magnetic field map for the 2 cm dia pole piece. The critical field line determined from this map is shown as a solid line, and the one obtained from the field map for a standard pole piece is shown dotted. Comparison of these lines shows the standard pole piece would result in an improved primary electron distribution because it would give greater primary electron densities and hence increased ionization probabilities near the outer radii of the thruster. The 2 cm diameter pole piece, producing the indicated critical field line, would therefore be expected to yield a lesser maximum utilization. Figure 15 shows the primary electron distribution in a main discharge chamber with a 2 cm diameter pole piece. This figure confirms the above theory in that primary electron density drops off substantially in the radial direction. In

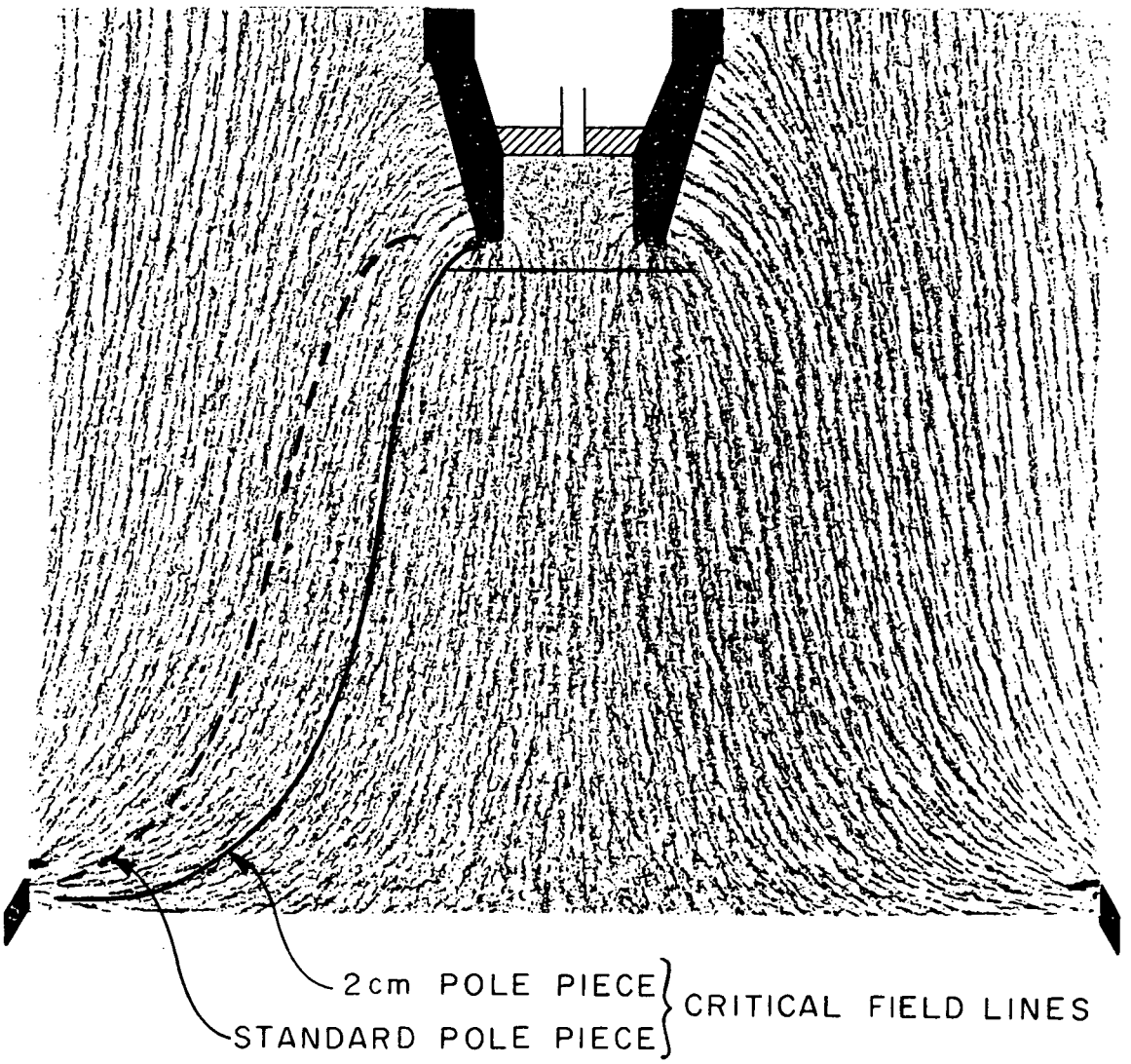

FIGURE 14. MAGNETIC FIELD MAP
(2 CM DIA. POLE PIECE)

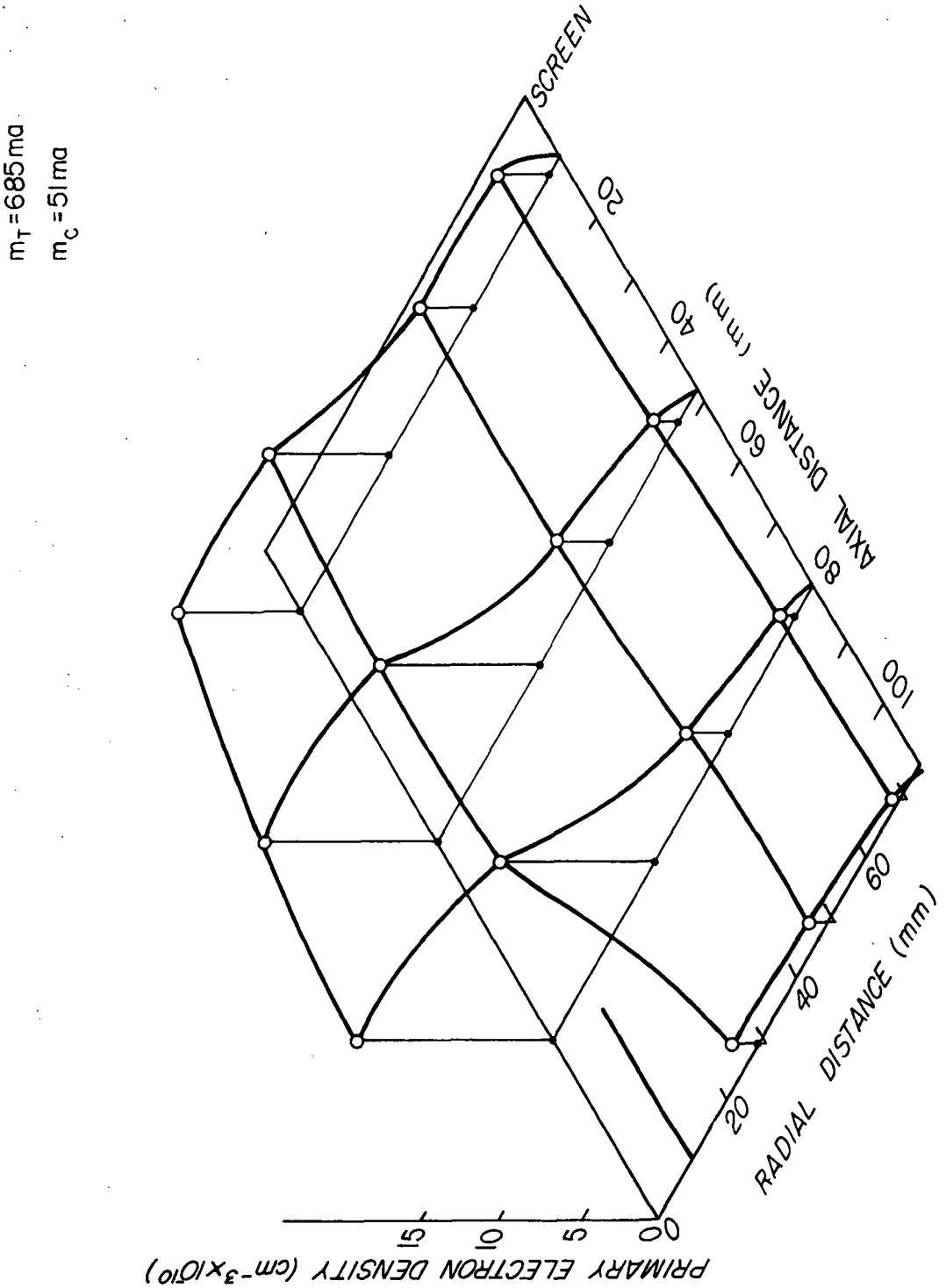

FIGURE 15. PRIMARY ELECTRON DENSITY CONTOUR
(2CM DIA. POLE PIECE)

contrast figures 9a and 10a show the contour observed with the standard pole piece, and it is seen to be quite flat in the region near the screen grid. It is concluded that retention of the small cathode discharge region is desirable to effect stable thruster operation over a wider range of arc voltage conditions and at lower cathode flows so long as it does not necessitate any undesirable variation in the shape of the magnetic field in the main discharge region.

High Perveance Grid Studies

Initial tests conducted on the 15 cm thruster employed flat accel and screen grids maintained at -1.6 kv and +1.6 kv respectively. These values were used in an effort to reduce specific impulses below the SERT II value and at the same time operate at a beam current level near 375 ma. Initial tests showed poor performance at flow rates near 440 ma total. This poor performance was found to be due to excessive ion and electron densities which were due in turn to an insufficient beam current. It was decided at this point to increase the high voltages to +3.4 kv on the screen and -1.7 kv on the accel grid with the idea that the grid perveance could eventually be increased so the same beam current could be drawn at lower grid voltages.

The final effort to achieve a 375 ma beam current at a low specific impulse involved the installation of high perveance, dished grids provided by NASA Lewis. With the dished grids the grid spacing could be reduced from 0.254 cm used on SERT II to 0.079 cm. The accelerator and screen grid potentials were then reduced to -0.5 kv and +1.0 kv respectively. With the close grid spacing the thruster could be operated at considerably

higher total flows than had been possible previously and throttling over a wide flow range was therefore possible. Figure 16 presents performance curves obtained with the dished grids at a high and a low total flow rate. These curves contain data which includes a beam current variation from 60 ma to 600 ma. Again, the maximum utilization indicated by these curves is lower than it should be. This is due to the 2 cm dia pole piece used in the tests which was discussed in the preceeding section.

Based on this work it has been concluded:

1) Extension of the cathode pole piece to increase the radial component of the magnetic field does not improve thruster performance.
2) Reducing the dimensions of the cathode pole piece facilitates stable operation of the 15 cm thruster over wider ranges of arc voltage and propellant flow rate. Such changes must be made with careful attention to their effect on the critical field line in the main discharge chamber. This field line should be positioned such that primary electrons are not confined near the thruster centerline.
3) The use of high perveance dished grids facilitates 15 cm thruster operation over a beam current range of at least 60 ma to 600 ma. Testing at higher beam currents is presently limited only by the obtainable flow rate through the main vaporizer.

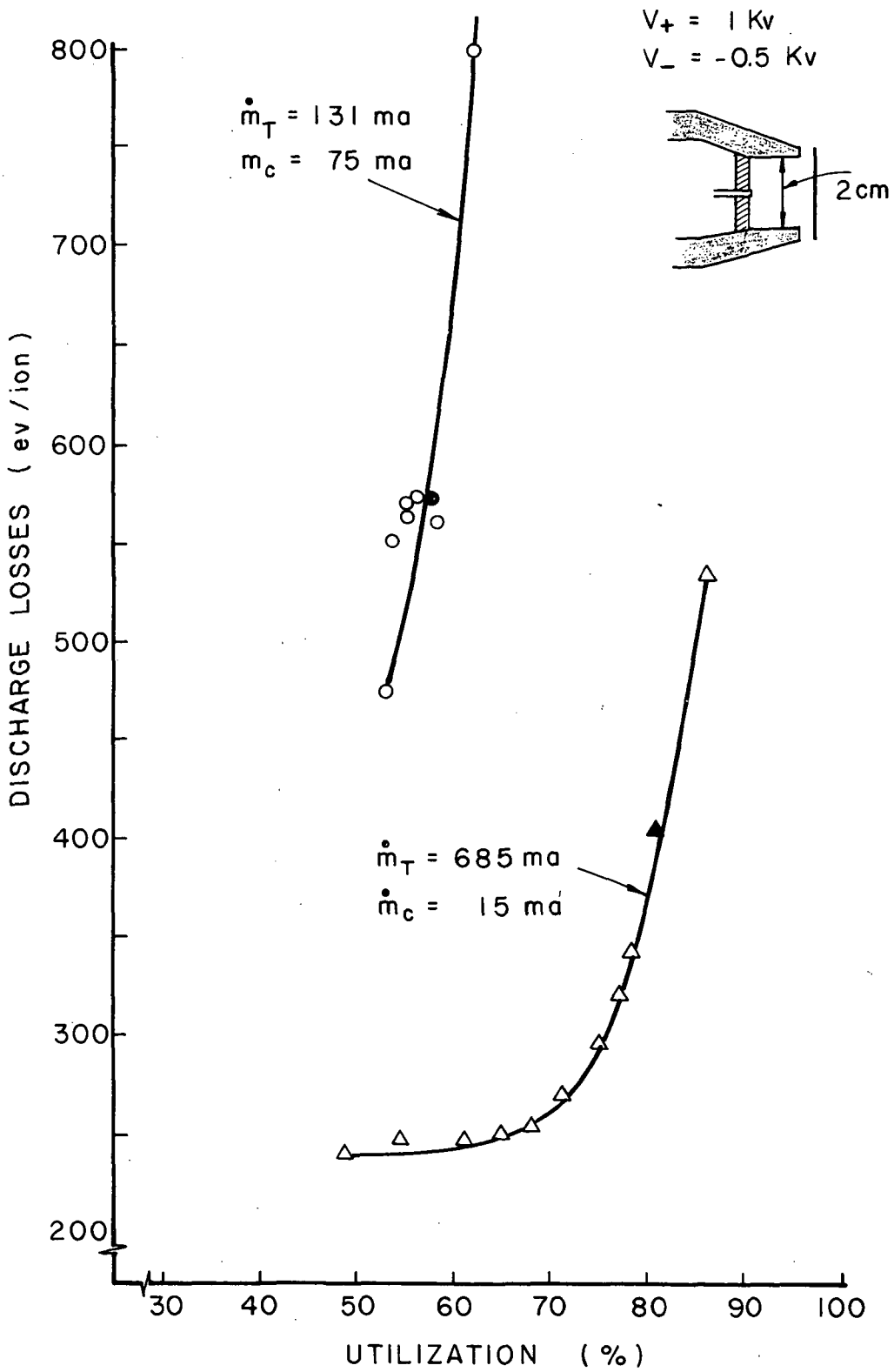

FIGURE 16. THRUSTER PERFORMANCE WITH DISHED GRIDS

STUDIES OF THE BAFFLE APERTURE REGION

Typical cathode discharge region plasma property contours measured in the 15 cm thruster with standard SERT II cathode discharge region are presented in Figure 17. The plots show electron density (n_e), electron temperature (T_e) and plasma potential (ϕ_p) on a plane passing through half of the discharge region and the thruster centerline. Axial position on these figures is measured from the tip of the cathode pole piece. The upper plot shows the electron density drops from about 4×10^{11} cm^{-3} in the vicinity of the cathode-keeper to about 5×10^{10} cm^{-3} near the baffle aperture, while the lowest plot shows plasma potential rises from 13 v in the vicinity of the cathode-keeper to near 25 v at the baffle aperture. The potential gradient vector, which proceeds in the direction of maximum slope, can be seen to lie in the general direction of a line joining the cathode and baffle aperture. The iron filing map of Figure 18a shows the magnetic field lines in the cathode regions corresponding to Figure 17. In the baffle aperture region these field lines are seen to be approximately perpendicular to the potential gradient vector mentioned above. This observation agrees with the more detailed study of Wells[9] who also notes the Hall parameter near the baffle aperture is considerably greater than unity. This means the baffle aperture is a region of large azimuthal electron drift, and this in turn provides an explanation for the abrupt increase in electron temperature at the baffle aperture which can be seen in the middle sketch of Figure 17. The Langmuir probe trace at the baffle aperture actually shows the plasma becomes non-maxwellian at this location, but with probe trace analysis assuming a maxwellian distribution, the energy input associated with this drift velocity manifests itself as an

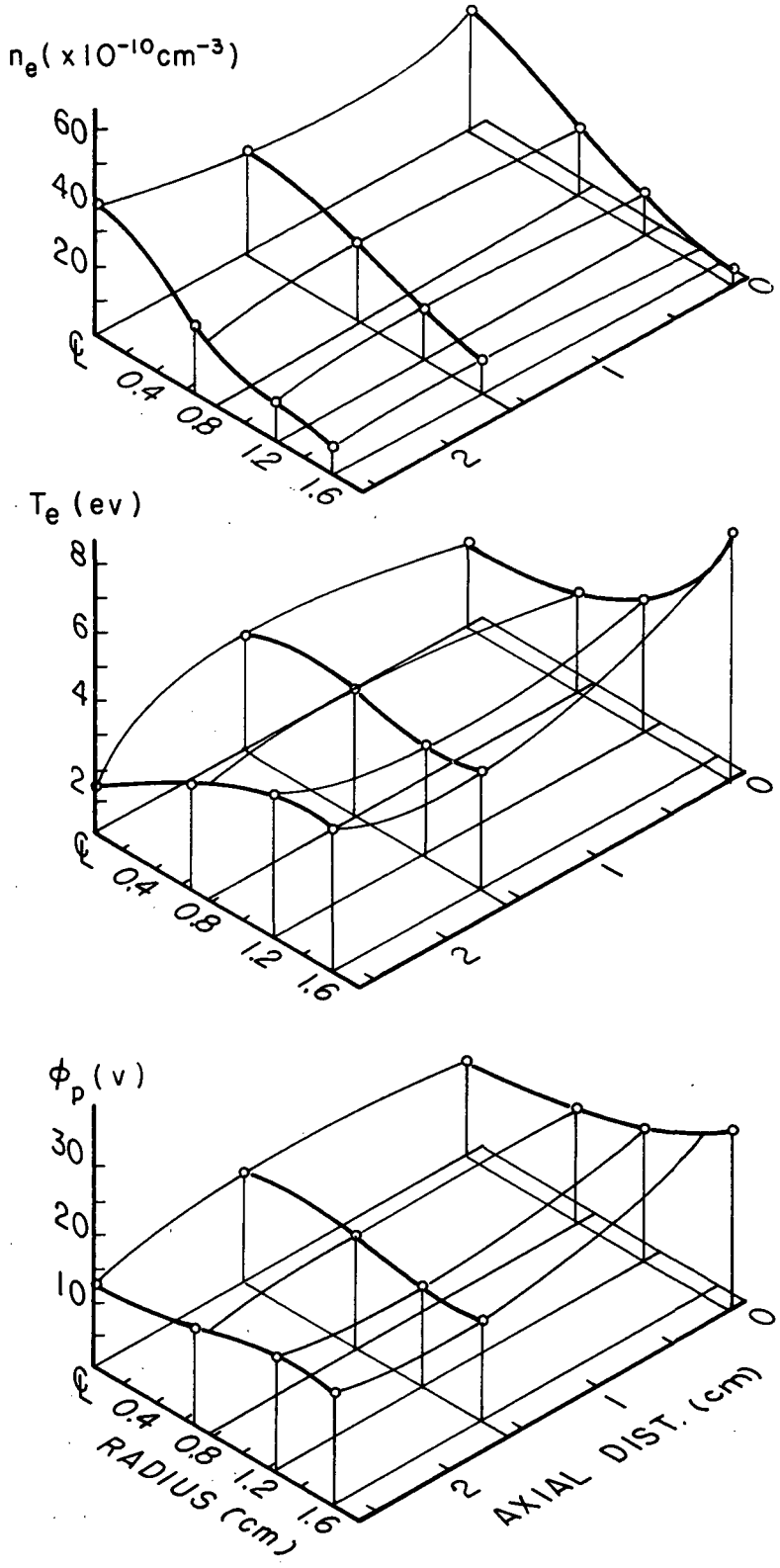

FIGURE 17. CATHODE REGION PLASMA PROPERTIES

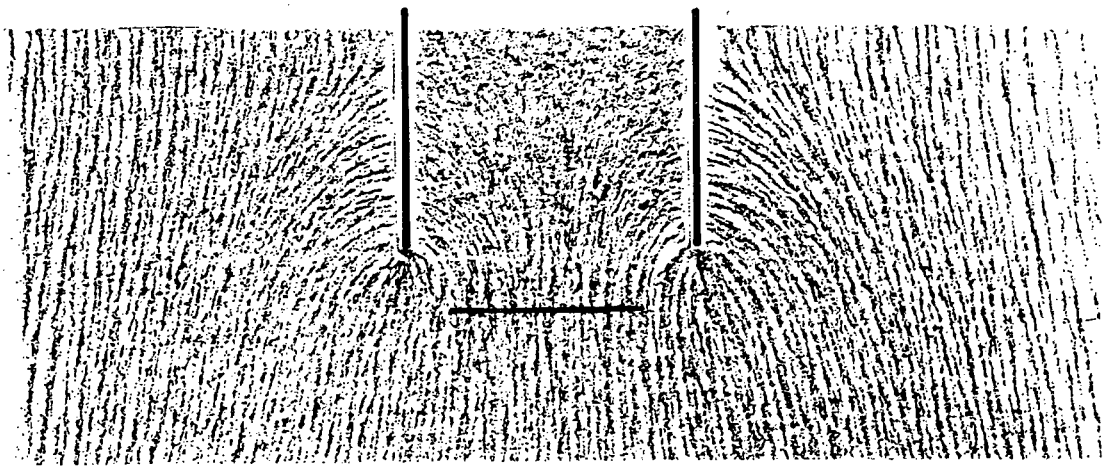

(a) STANDARD SERT II POLE PIECE-BAFFLE

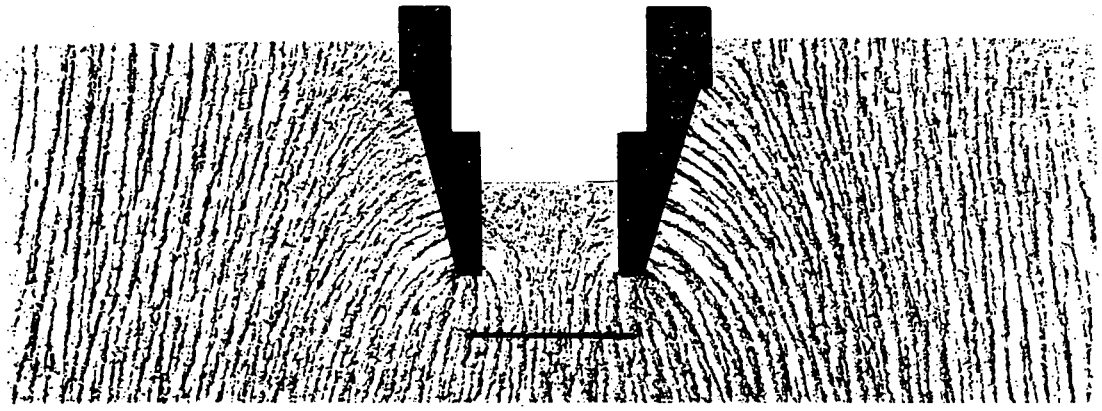

(b) 2cm DIA. POLE PIECE – BAFFLE

FIGURE 18. CATHODE REGION MAGNETIC FIELD MAPS
(15 CM THRUSTER)

increase in electron temperature. Cathode discharge region properties were observed to be similar over a range of operating conditions (cathode and main flow rates, arc voltages, keeper currents and cathode heater powers).

The condition mentioned above wherein the potential gradient vector is perpendicular to the magnetic field lines were found to be a requirement for proper thruster operation in general. Figure 18b shows the 2 cm dia pole piece and baffle on the 15 cm thruster where it can be seen electron flow across magnetic field lines is required. Figure 19 displays magnetic field maps obtained on the 20 cm thruster in the tests conducted during the previous report period where sleeves were inserted within the cathode pole piece to confine the cathode discharge dimensions[4]. The field line map of Figure 20a shows the baffle aperture magnetic field lines when a 3.5 cm dia cathode pole piece confined the cathode region plasma. In all of these 20 cm configurations too, the magnetic field lines are essentially perpendicular to the electric field vector and they therefore obstruct electron flow through the baffle aperture. This condition would also appear to exist in magnetic baffle thrusters[10].

The bottom and middle portions of Figure 20 show the configuration of the 2 cm dia cathode discharge region tested on the 20 cm thruster along with the associated magnetic field map. Two baffle configurations are also indicated. Electrons must migrate across the field lines in the baffle region with either configuration. Thruster operation with axial injection at a total flow of 465 ma was characterized by high cathode flow rates ($\dot{m}_c \approx 100$ ma) and a peaked ion beam current density profile (beam

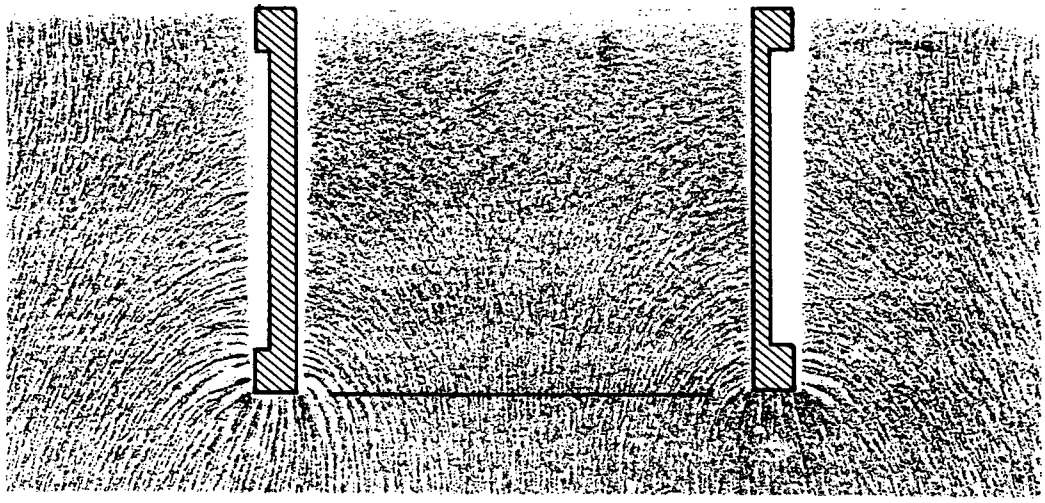

(a) STANDARD POLE PIECE-BAFFLE

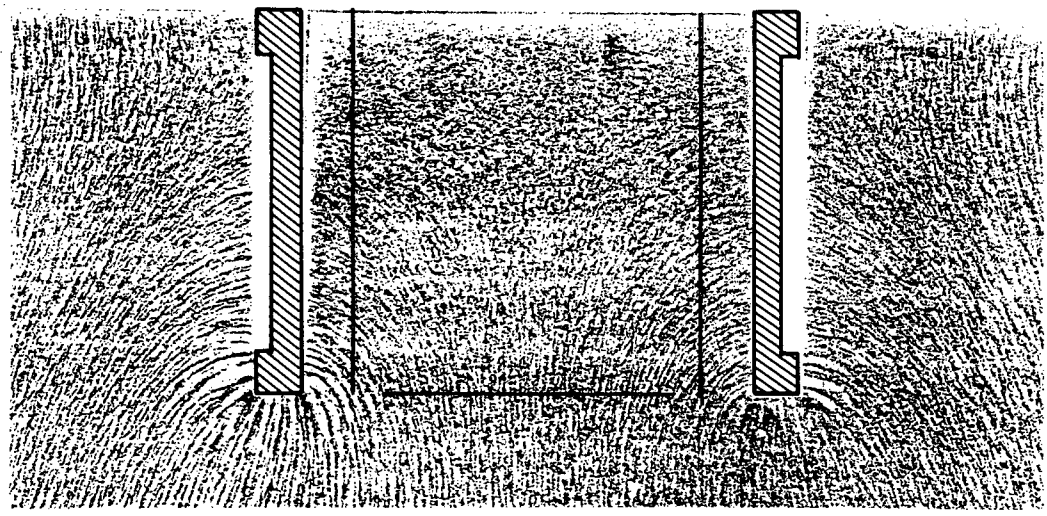

(b) 4.92 cm DIA. SLEEVE INSTALLED

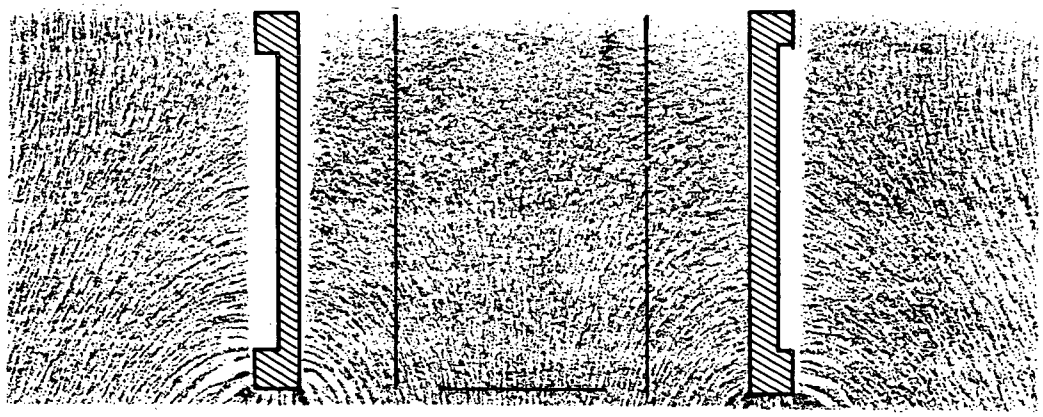

(c) 3.5 cm DIA. SLEEVE INSTALLED

FIGURE 19. CATHODE REGION MAGNETIC FIELD MAPS
(20 CM THRUSTER)

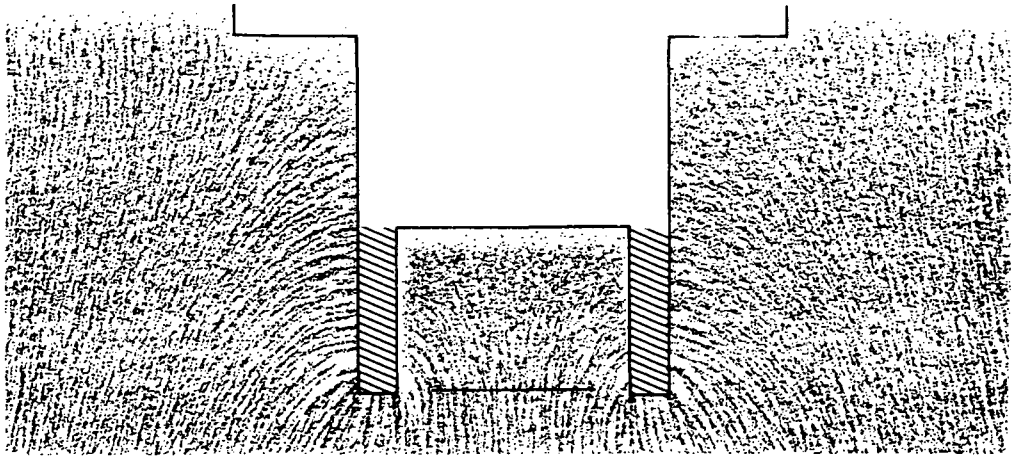

A. 3.5 cm DIA. CATHODE POLE PIECE

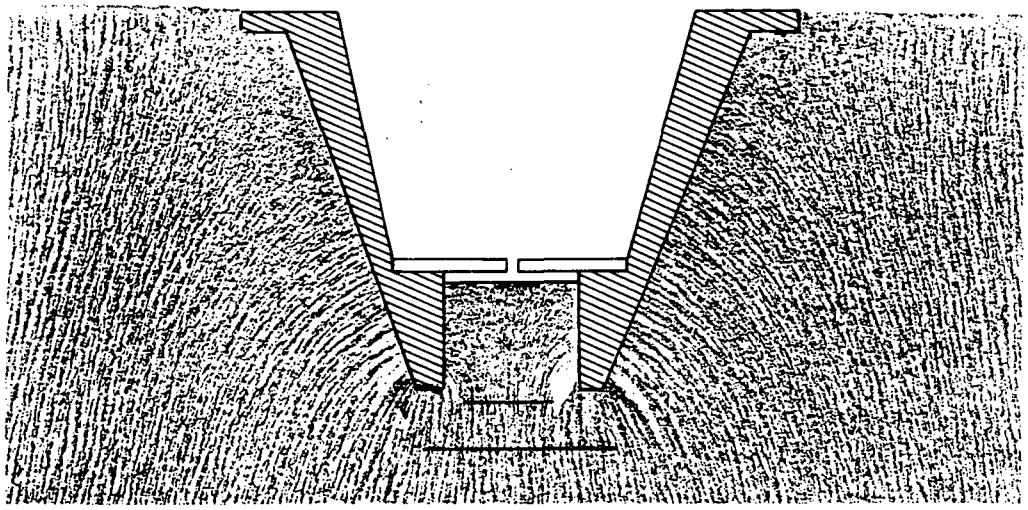

B. 2.0cm DIA. CATHODE POLE PIECE

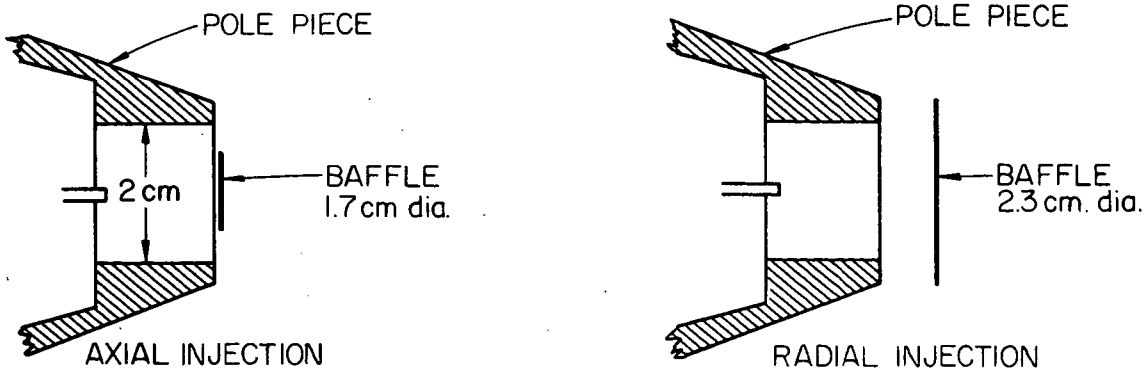

C. 2 cm DIA POLE PIECE BAFFLE CONFIG.

FIGURE 20. CATHODE REGION MAGNETIC FIELD MAPS
(20 CM THRUSTER)

flatness parameter $\varepsilon^{*} \approx 0.21$). Largely because of the peaked ion beam profile, the larger baffle was installed, and the resulting radial injection configuration effected a reduction in cathode flow rate ($\dot{m}_c \approx 35$ ma) and a flattening of the ion beam profile ($\varepsilon \approx 0.38$). Performance obtained with the small discharge region (2 cm dia) and radial electron injection is compared with that obtained with the 3.5 cm dia cathode region[4] in Figure 21 for a total flow of 465 ma. Performance is seen to be comparable with these two cathode region configurations.

At higher total flows in the 20 cm thruster the 2 cm dia cathode pole piece results in a performance degradation which is a result of a reduction in the maximum obtainable propellant utilization efficiency. This same behavior was observed with a 2 cm dia pole piece in the 15 cm thruster. In both cases this reduction in maximum propellant utilization was accompanied by a more peaked ion beam profile than the one observed with larger diameter pole pieces. These observations suggest primary electrons are not reaching the outer radii of the thruster and that neutrals are escaping these regions without being ionized. As pointed out in the previous section (Figure 14) this is probably due to improperly oriented critical magnetic field lines in the 2 cm cathode pole piece configuration. One might consider it possible to improve this condition somewhat by pulling the baffle back closer to the cathode pole piece thereby forcing electrons out further onto field lines which pass through the outer radii in the thruster. The effect of moving the baffle axially in order to accomplish this on the 15 cm thruster is examined in Figure 22. With the thruster

* This parameter was proposed by Knauer[6]. It is defined as the ratio of average to maximum beam current density for a given profile, and it was referred to as perveance utilization. It is referred to as the beam flatness parameter here because the term is considered more descriptive.

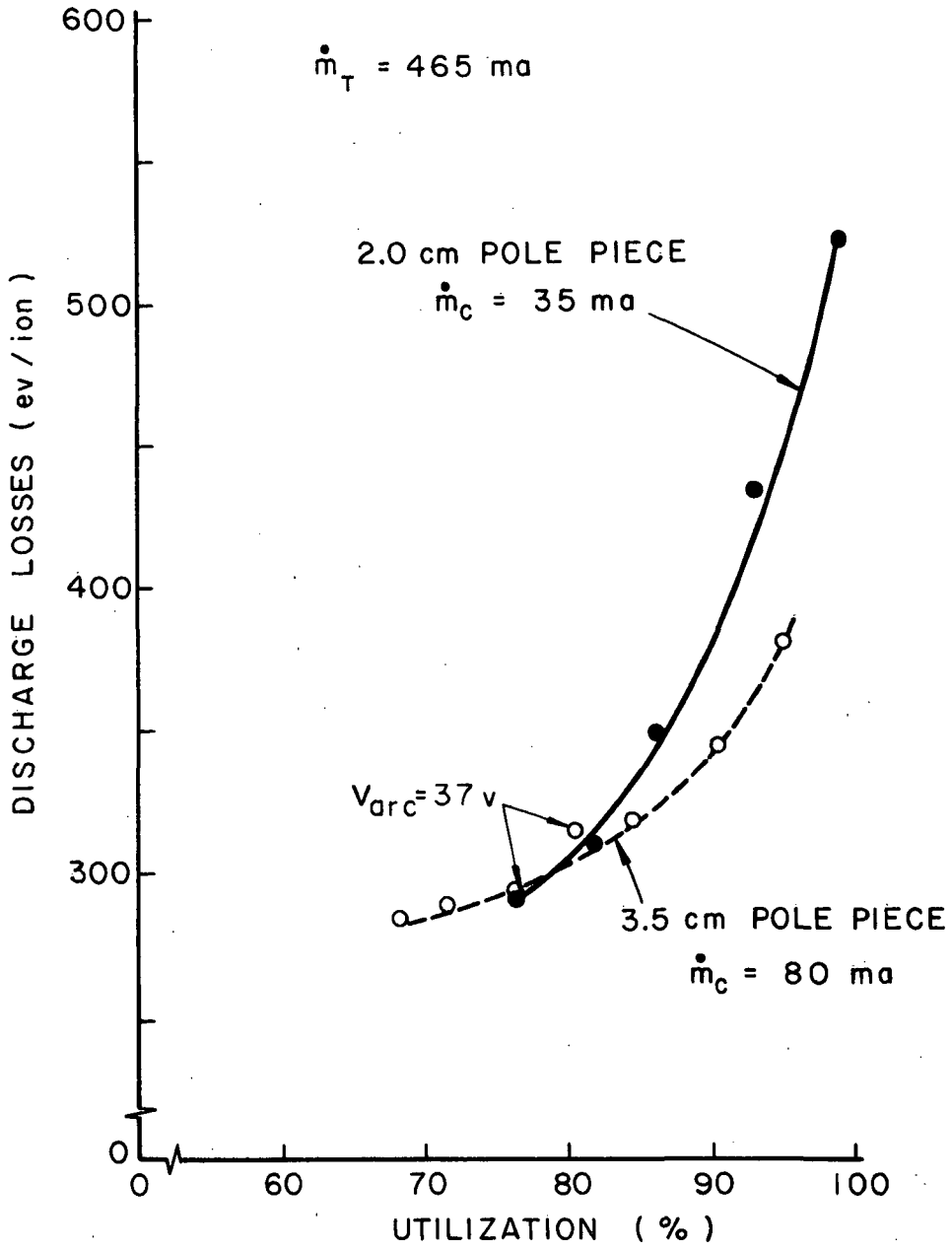

FIGURE 21. EFFECT OF POLE PIECE DIA. ON PERFORMANCE (20 CM THRUSTER)

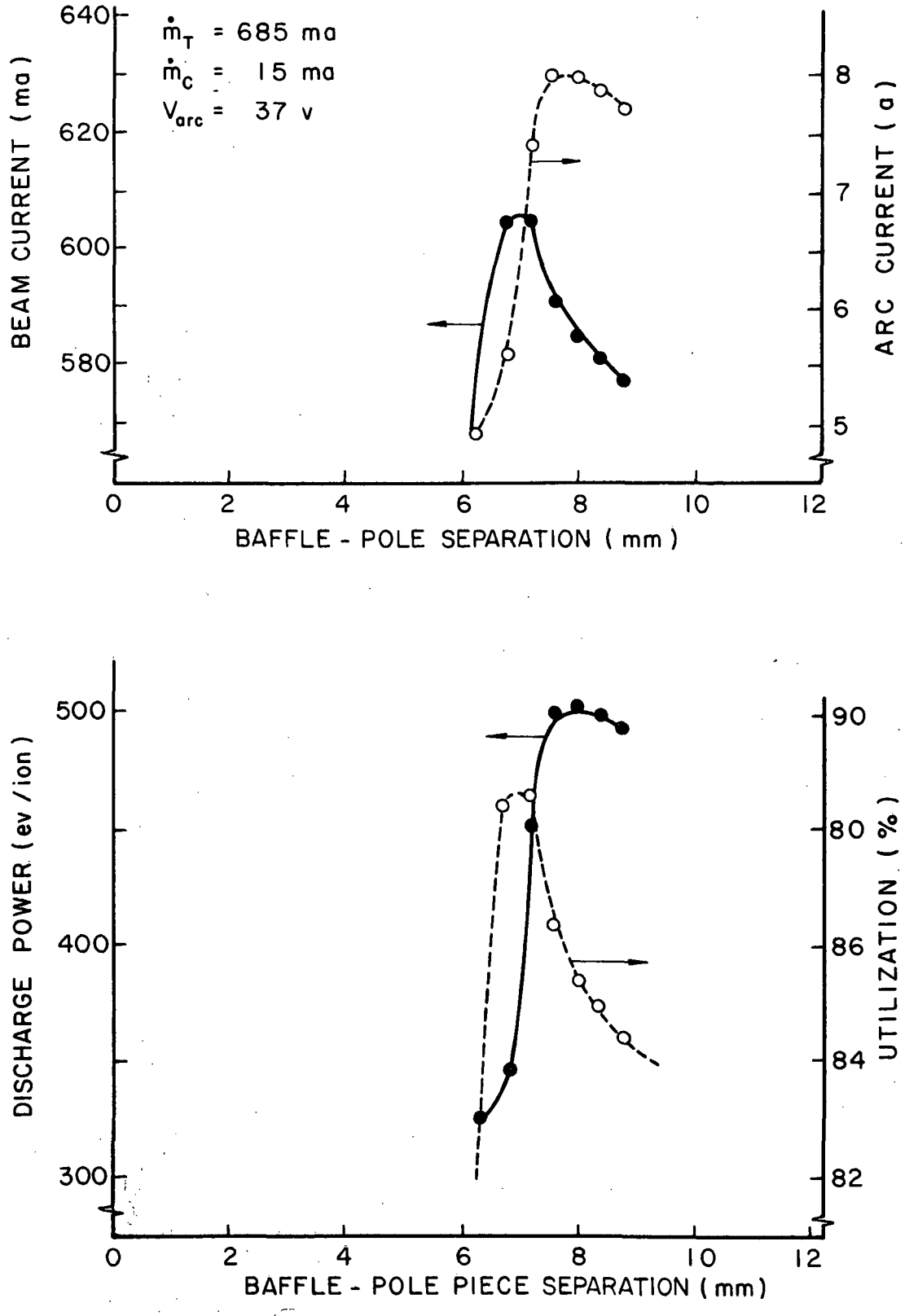

FIGURE 22. EFFECT OF BAFFLE POSITION
(15 CM THRUSTER)

operating at a fixed arc voltage and flow rate conditions the baffle aperture was reduced by moving the baffle toward the pole piece. Initially this caused an increase in arc current and beam current followed by a decrease in arc current and a further increase in beam current. One would ordinarily expect arc current to decrease as aperture area was decreased, and one would certainly not expect beam current to increase when arc current was decreasing unless primary electrons were being distributed more effectively in the discharge chamber as suggested above. The plots on the lower half of Figure 22 show how the variations in arc and beam current affect discharge losses and utilization efficiency.

The following conclusions suggest themselves:

1) Electron flow across magnetic field lines of force is essential to cathode discharge operation in the arc voltage range of interest (>35 v).

2) The baffle aperture must be located in such a way that it introduces primary electrons onto magnetic field lines which reach the outer regions of the discharge chamber over a significant fraction of its length without allowing electron flow directly to the anode.

ION DENSITY PROFILE - BEAM CURRENT DENSITY PROFILE CORRELATION STUDY

In order to maximize the thrust from an electrostatic thruster operating at an ion beam current density set by the desired grid lifetime, the beam current density profile should be made as flat as possible (i.e. the beam flatness parameter[6]--the ratio of average ion current density to maximum ion current density--should be as near unity as possible). The following study shows there is a high correlation between the beam current density profile at the accelerator grid, and the ion density profile at the screen grid. This implies the ion beam current profile can be flattened by flattening the ion density profile within the thruster.

The study was conducted using the 15 cm thruster operating over the range of beam current and high voltage conditions and with flat and dished grids as indicated in Table II. The mean ion beam current density profile at the accelerator grid was determined by sweeping a Faraday probe described in reference (4) through the beam at four axial locations (1.27 cm, 2.54 cm, 3.81 cm, 5.04 cm aft of the plane tangent to the center of the accel grid) and extrapolating the resulting data at several radial positions back to the plane tanget to the center of the grid. Similarly, Langmuir probe data were obtained at nine radial locations on at least two axial locations in the discharge chamber (11 mm and 23 mm from the plane of contact of the screen grid and anode pole piece), to permit determination of the ion density profiles and then extrapolation of these profiles to the plane of contact mentioned above. In tests 6 through 9 of Table II sweeps were made at 3 axial locations (11 mm, 17 mm and 23 mm from the plane of contact). The current and ion density profiles at the screen grid were normalized using, respectively, the maximum current and ion densities

corresponding to the profile in question.

Tests 2 and 5 which were conducted at essentially the same conditions provide an indication of the variation in correlation coefficient which might be expected in the study. The variation is considered to be due primarily to errors in Langmuir probe data evaluation.

Table II
15 cm Thruster Operation Conditions for
Beam Current - Density Correlation Study

Test No.	Beam Current	High Voltage Pos.	High Voltage Neg.	Thruster Configuration	Correlation Coefficient[11]
1	0.354a	3.4 kv	-1.7 kv	SERT II	.971
2	0.171a	3.4 kv	-1.7 kv	SERT II	.904
3	0.148a	1.5 kv	-0.5 kv	SERT II	.911
4	0.235a	3 kv	-1.5 kv	SERT II	.983
5	0.178a	3.4 kv	-1.7 kv	SERT II	.971
6	0.149a	3.4 kv	-1.7 kv	2 cm dia. Cathode Pole Piece	.970
7	0.356a	3.4 kv	-1.7 kv	2 cm dia. Cathode Pole Piece	.988
8	0.071a	1 kv	-0.5 kv	2 cm dia. Pole Piece Dished Grids	.963
9	0.128a	1 kv	-0.5 kv	2 cm dia. Pole Piece Dished Grids	.964

Correlation Coefficient for all data = 0.945

A typical comparison between the resulting profiles is presented as Figure 23 (Test 3 of Table II). A linear regression analysis[11] was conducted using the ion density data points shown as solid symbols on the typical plot (Figure 23) and the values of beam current density at the same radial

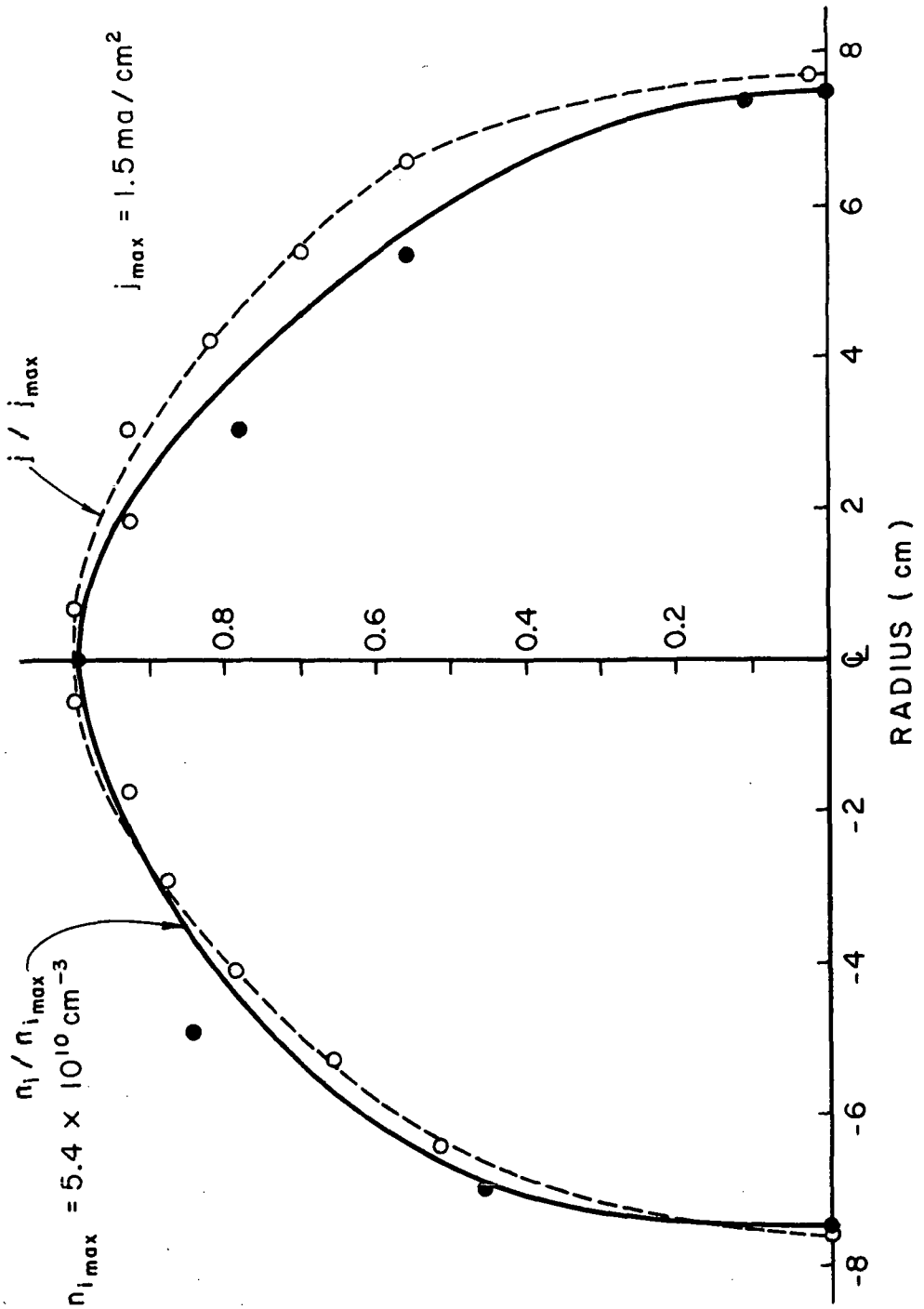

FIGURE 23. BEAM CURRENT - ION DENSITY TYPICAL SHAPE CORRELATION

location (dotted line). The resulting correlation coefficients for each set of data, as well as the correlation coefficient for the pooled data (0.945) are given in Table II. Since the data were collected over a range of flow distribution, beam current and high voltage conditions and the correlation remained high, there is a high probability that beam current profile is determined by the ion number density profile and is dependent on other thruster parameters only insofar as they affect this profile.

MAXIMUM PROPELLANT UTILIZATION IN HOLLOW CATHODE THRUSTERS

In a recent study Kaufman[8] showed the neutral loss rate from a 10 cm thruster which employed a refractory metal cathode was independent of total flow through the thruster. The refractory metal cathode was used in this study to avoid "the uncertainty in propellant utilization that can occur when an oxide cathode is inadvertantly overheated, and the effect of localized propellant concentration associated with a hollow cathode".[8]

In order to determine if the fixed neutral loss rate conclusion could be applied to hollow cathode thrusters on the average, the neutral loss rates were calculated for all data obtained to date with the 15 cm thruster and the 20 cm thruster. Data were obtained for both thrusters at 37 v arc voltage and a fixed surface area to volume ratio for the primary electron region. These data are presented in Figure 24 for the two thrusters. The data show considerable scatter as Kaufman predicted, but the mean data points suggest a nearly constant neutral loss rate in the 15 cm thruster. The 20 cm thruster data show a decrease in neutral loss rate as total flow is increased. The reason for this is not known, but it may be due to changing primary electron region surface area to volume or primary to secondary electron density ratios.

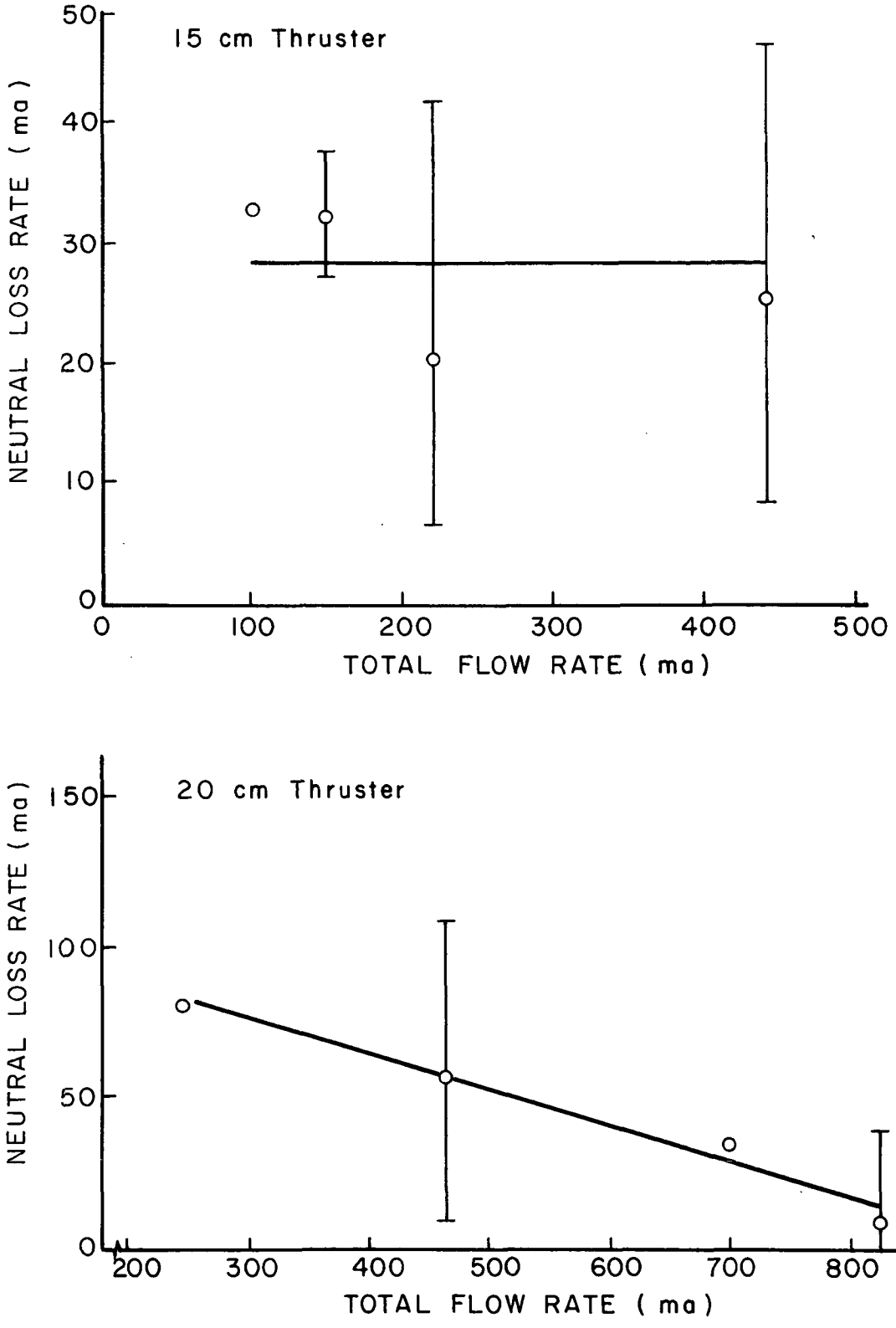

FIGURE 24. EFFECT OF TOTAL FLOW RATE ON NEUTRAL LOSS RATE

BASE LINE BEAM ION PRODUCTION COST

If one assumes all of the energy deposited in the main discharge chamber is deposited in the plasma ions; that the average production cost of a plasma ion is C_I (ev/ion) and that these ions, generated within a primary electron region of surface area A_{total} (m^2), are lost across this surface at a uniform current density j (ion/sec m^2); the total power supplied to the main discharge is:

$$P_T = j\ C_I A_{total} \quad \text{(ev/sec)} \tag{1}$$

The ion beam current then through a grid system of open area A_o (m^2) would be given by

$$I_B = j\ A_o \quad \text{(ion/sec)}. \tag{2}$$

Combining these two equations the base line beam ion cost P_B is given by

$$P_B = \frac{P_T}{I_B} = \frac{C_I A_{total}}{A_o} \quad \text{(ev/ion)}. \tag{3}$$

Experiments conducted with a moveable cathode pole piece sleeve made it possible to vary the total area (A_{total}) by varying the area of the surface of revolution of the critical field line. The extent of this variation can be seen in Figures 3, 4 and 5 which are magnetic field maps obtained with the pole piece sleeve extended various amounts. Discharge power supplied to the main discharge was evaluated at the knee of the performance curves obtained at each sleeve position by using:

$$P_B = \frac{(V_{arc} - V_{keeper})\ I_{arc}}{I_{beam}}$$

The difference between arc and keeper voltage was used as a means of subtracting off the beam ion cost associated with the cathode discharge operation which was not a part of this simple analysis. The correlation between beam ion cost and area ratio A_{total}/A_o is shown in Figure 25. The data show considerable scatter because of the range of cathode and main flow rates considered, but the distribution of the beam ion cost data around the mean point shown was symmetric and the results are considered statistically significant. The slope of the line through the data (38 ev/ion) corresponds to the plasma ion production cost C_I of equation (3). This value compares favorably with the range 20 - 40 ev/plasma ion predicted by Masek[13]. The P_B intercept (40 ev/ion) is also seen to be quite small, and it therefore provides additional confirmation of this simple model.

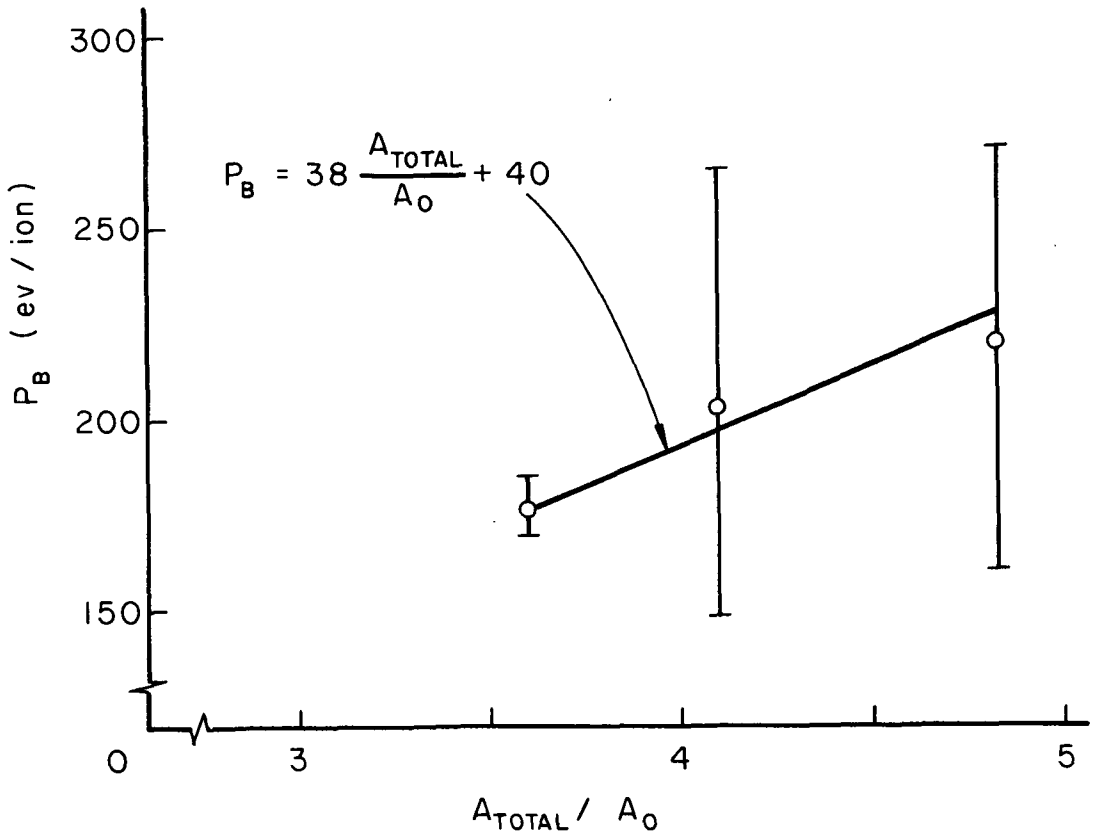

FIGURE 25. EFFECT OF PRIMARY ELECTRON REGION TOTAL SURFACE AREA TO BEAM EXTRACTION AREA RATIO ON BASELINE DISCHARGE LOSSES

NEUTRAL BALANCE MODEL FOR THE CATHODE DISCHARGE REGION

The neutral atom density in the cathode discharge region of the thruster (which affects electrical conductivity there) is generally controlled by adjustments in the propellant flow rate through the hollow cathode. A reduction in cathode flow rate at a fixed arc voltage generally results in an increase in arc current. In recent tests[1] however a reduction in cathode flow rate and a concomitant increase in main flow rate to hold a fixed total flow rate resulted in an increase in arc current. This suggested that conditions in the main discharge might also affect atomic density in this region. The following analysis provides an expression for the atomic density in the cathode discharge region and indicates cathode flow rate has the dominant effect on this density.

The cathode and main discharge regions of the thruster are shown schematically in Figure 26 where the symbols to be used in this analysis are also defined. It is assumed that:

1) Neutral atom temperature is equal to the thruster wall temperature and is uniform throughout the thruster.
2) The Bohm criterion based on main discharge plasma properties in the baffle vicinity can be applied to determine the ion current through the baffle aperture.
3) Free molecular flow theory can be used to describe neutral flow through baffle aperture and grid areas.
4) Neutral back flow from the test chamber into the thruster is negligible.

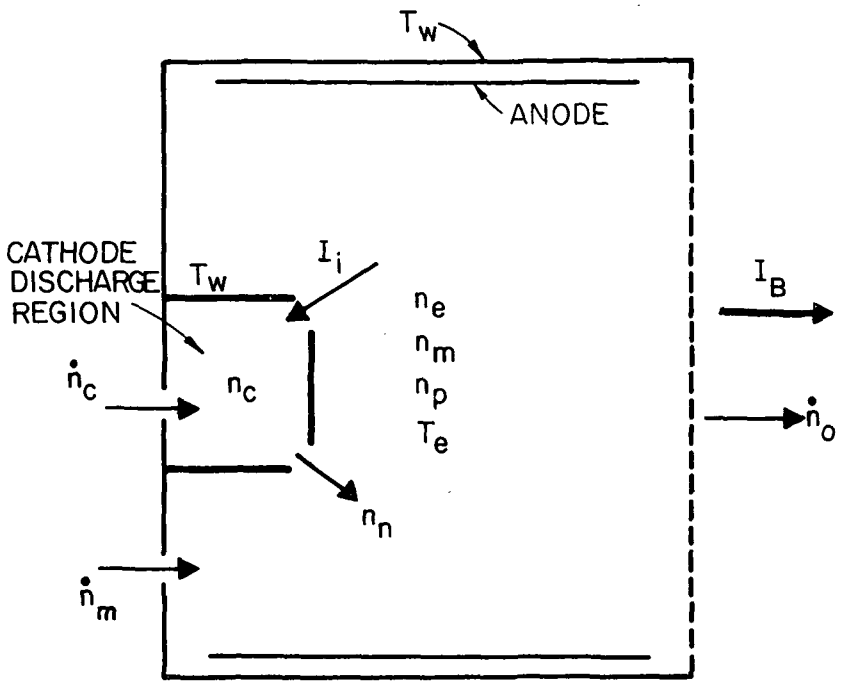

Neutral Balance Model

$\dot{n}_m$ = neutral flow rate into main discharge region (sec^{-1})

$\dot{n}_c$ = neutral flow rate into cathode discharge region (sec^{-1})

$\dot{n}_o$ = neutral flow rate from thruster (sec^{-1})

n_c = cathode region neutral density (m^{-3})

n_e = main region maxwellian electron density (m^{-3})

n_p = main primary electron density (m^{-3})

n_m = main neutral density (m^{-3})

T_e = main region maxwellian elec. temp. (°K)

T_w = wall temperature (°K)

I_B = beam current (amps)

I_i = ion current into cathode region from main region (amps)

$\dot{n}_n$ = net neutral flow rate from cathode to main region (sec^{-1})

FIGURE 26. NEUTRAL BALANCE MODEL

In the steady state, the net rate of outflow of neutrals from the cathode discharge region into the main discharge region ($\dot{n}_n$) is equal to the sum of the inflow rate of ions from the main discharge (I_i/e) and the inflow rate of neutrals through the hollow cathode ($\dot{n}_c$). "e" is the electron charge.

$$\dot{n}_n = \frac{I_i}{e} + \dot{n}_c \tag{4}$$

The net neutral outflow rate is determined from free molecular flow considerations by the difference between neutral outflow rate and the inflow rate from the main discharge.

$$\dot{n}_n = \frac{n_c A_B V_n}{4} - \frac{n_m A_B V_n}{4} = \frac{A_B V_n}{4} (n_c - n_m) \tag{5}$$

A_B is the baffle aperture area and V_n, the neutral velocity, is determined from kinetic theory by the wall temperature and is assumed to be the same in both regions.

$$V_n = \sqrt{\frac{8\ kT_w}{\pi\ m_o}} \tag{6}$$

"k" in this expression is the Boltzmann constant and "m_o" is the ion or neutral atom mass. The ion velocity determined by the Bohm criterion as modified by Masek to account for primary electrons is given by:[13]

$$V_i = \sqrt{\frac{k\ T_e(n_p + n_e)}{n_e m_o}} \tag{7}$$

Assuming charge neutrality and a uniform ion current density through the baffle aperture and employing the definition of ion current one obtains from (7):

$$\frac{I_i}{e} = A_B(n_p + n_e)\sqrt{\frac{k\ T_e(n_p + n_e)}{n_e m}} \tag{8}$$

It should be noted that the ion current from the cathode region to the main region is neglected here on the basis of the adverse potential gradient in the baffle aperture area. All of the quantities in equations 4 through 8 can be measured readily in an operating thruster except n_m. This quantity, the main region neutral density, is determined by an ion-neutral balance in the main chamber. That is

$$\dot{n}_c + \dot{n}_m = \frac{I_B}{e} + \dot{n}_o \tag{9}$$

where the neutral loss rate is given by

$$\dot{n}_o = \frac{n_m A_o V_n}{4} = \frac{n_m A_o}{4}\sqrt{\frac{8\,k\,T_w}{\pi\ m_o}} \tag{10}$$

A_o is the grid system open area, and a uniform neutral density in the main discharge region has been assumed in obtaining this equation.

Combining equations (4), (5), (6), (8), (9) and (10) one obtains:

$$n_c = 4\sqrt{\frac{\pi\, m_o}{8kT_w}}\left[\frac{\dot{n}_c + \dot{n}_m - I_B/e}{A_o}\right] + \frac{4\dot{n}_c}{A_B}\sqrt{\frac{\pi\, m_o}{8kT_w}} + (n_p + n_e)\sqrt{2\pi\,\frac{T_e}{T_w}\left(1 + \frac{n_p}{n_e}\right)} \tag{11}$$

The first term of this equation represents the contribution to the cathode region neutral density due to neutral back flow from the main discharge region, the second is the contribution due to the cathode flow rate, and the third is the contribution due to ion current flow from the main discharge.

The following values of the parameters in equation (11) were obtained in a 20 cm thruster and are considered somewhat typical.

$$\dot{n}_m = 0.395 \text{ a eq} = 2.47 \times 10^{18} \text{ sec}^{-1}$$

$$\dot{n}_c = 0.070 \text{ a eq} = 4.37 \times 10^{17} \text{ sec}^{-1}$$

$$I_B = 0.370 \text{ amp}$$

$A_B = 9.5 \times 10^{-5}\ m^2$

$A_o = 2.2 \times 10^{-2}\ m^2$

$n_e = 1.7 \times 10^{17}\ m^{-3}$

$n_p = 1.7 \times 10^{16}\ m^{-3}$

$T_e \approx 3\ ev = 34{,}800°K$

$T_w \approx 500°K$

$m_o = 3.3 \times 10^{-25}\ kg$

Substitution into equation (11) yields

$$n_c = 0.47 \times 10^{18} + 80 \times 10^{18} + 4 \times 10^{18} = 84.5 \times 10^{18}\ m^{-3}$$

From this result one can see for this typical case 94.7% of the neutrals in the cathode discharge region come from the hollow cathode, 4.7% are due to ion backflow from the main discharge and 0.6% are due to neutral backflow from the main discharge.

DOUBLE ION PRODUCTION

Double ion number densities in mercury electron bombardment ion thrusters have been assumed negligible at electron energies below about 35 ev because of the relatively low cross sections for double ionization of neutral mercury at these energies[14]. Recent thruster plasma studies present spectroscopic and mass spectrometer measurements which suggest the double ion densities are considerably higher at these low energies than anlysis based on this reaction would suggest [12, 15]. An alternative reaction which might account for the higher than anticipated double ion densities is:

$$Hg^{+} + e^{-} \rightarrow Hg^{++} + 2e^{-} \tag{12}$$

Although the cross sections for this reaction have not been measured, they can be estimated using the Gryzinski expression[16].

$$\sigma(E) = \sum_i \frac{6.56 \times 10^{-14}}{U_i} \left[\frac{1}{x_i} \left(\frac{x_i - 1}{x_i + 1} \right)^{3/2} \left(1 + \frac{2}{3} \left\{ 1 - \frac{1}{2x_i} \right\} \ell n[2.7 + (x_i - 1)^{1/2}] \right) \right] \tag{13}$$

where $\sigma(E)$ is the cross section in cm^2 for ionization by an electron of energy E in units of electron volts, U_i is the ionization potential in ev for the i^{th} bound electron of the target atom or ion, and $x_i \approx E/U_i$.

The generation rate for double ions in a volume V of uniform ionizing electron density n_e, electron velocity v_e and single ion density n_+ is given by

$$R_g = n_+ \, n_e \, v_e \sigma_+^{++} \, V \tag{14}$$

where σ_+^{++} is the cross section for the reaction (12). The double ion loss rate is controlled by recombination presumed to occur after ions have

crossed primary electron region boundaries and is given by:

$$R_{\ell} = n_{++} v_{++} A \tag{15}$$

where n_{++} is the double ion density, v_{++} is the double ion velocity and A is the surface area bounding the region. Equating these on the basis that the thruster is operating in the steady state, one obtains:

$$n_{++} = \frac{n_+ n_e v_e \sigma_+^{++} V}{v_{++} A} \tag{16}$$

If one assumes the predominant single ion loss rate is also recombination at boundaries then for the production of single ions from neutrals one has the following similar expression:

$$n_+ = \frac{n_o n_e v_e \sigma_o^{+} V}{v_+ A} \tag{17}$$

Taking the ratio of equations (16) and (17), multiplying by (n_+/n_o), and recognizing the single and double ion temperatures are about equal $(v_+ \approx v_{++})$ one obtains:

$$\frac{n_{++}}{n_o} = \left(\frac{n_+}{n_o}\right)^2 \frac{\sigma_+^{++}}{\sigma_o^{+}} \tag{18}$$

The cross sections required in this equation can be obtained from the Gryzinski expression (13). For neutral mercury the outer electrons which must be considered in the summation of this equation are the two 6s electrons (U = 10.43 ev)[17] and the ten 5d electrons (U = 16.7 ev)[17]. For singly ionized mercury the remaining 6s electron has an ionization potential of 18.75 ev[17], but the ionization potential for the 5d electrons in this configuration is not known. It has been estimated for this analysis to be 24 ev which is the sum of the ionization potential of Hg^+

(18.75)[17] and the energy required to remove a 5d electron of Hg^{++} into the 6s configuration (5.3 ev)[17]. The cross sections obtained using these values are given in Figure 27 for the single and double ionization reactions of neutral and singly ionized mercury respectively. Experimental values for the single ionization cross section (σ_0^+) could have been used in equation (18), but the theoretical value was used to insure consistency with the double ion cross section.

Milder and Sovey[12] obtained their double ion fractions (n_{++}/n_0) from spectroscopic data on a thruster operating at a fixed ion beam current. Their data show the single ion fraction (n_+/n_0) remained constant as arc voltage (and hence primary electron energy) was varied under this condition. If one assigns a single ion fraction of 0.1 as typical of an operating thruster, the double ion fraction calculated from equation (18) and the Milder-Sovey double ion data lend themselves to direct comparison. Figure 28 presents this comparison as a function of ionizing electron energy, with the thruster centerline double ion fractions superimposed as triangles on the theoretical curve. The thruster centerline double ion data[12] were selected from the experimental data on the basis that density gradients are minimal there and hence these results are most compatible with the assumptions of the mathematical model.

The data of Figure 28 show electrons can be supplied by this ionization mechanism at energies below 35 volts, but the observed double ion fraction is considerably higher than the theoretically predicted values. This discrepancy is probably due to one or more of the following:

1) The assumed single ion fraction (n_+/n_0) is too low.
2) Production of double ions from atoms and/or single ions in excited states is significant.

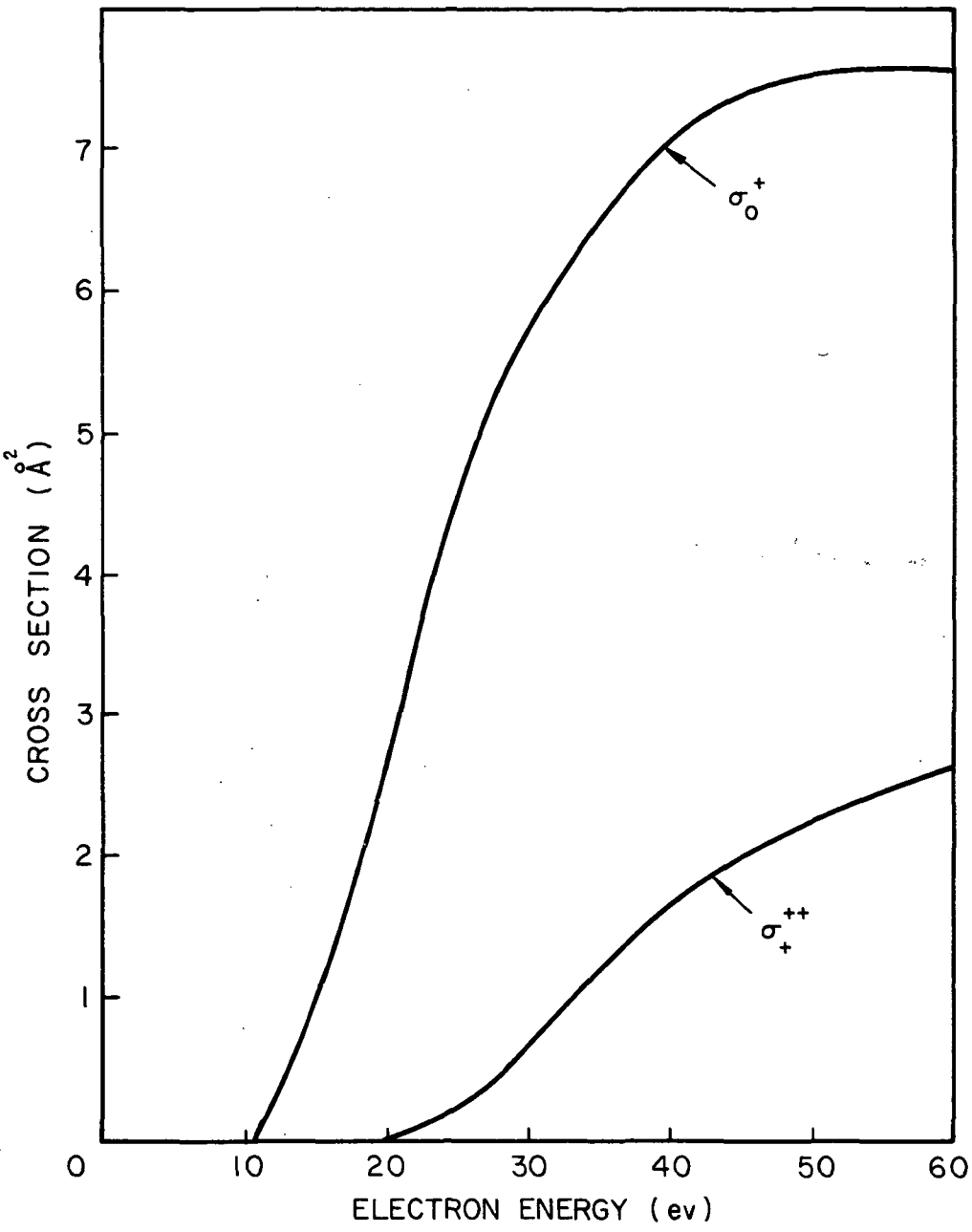

FIGURE 27. THEORETICAL MERCURY IONIZATION CROSS SECTIONS

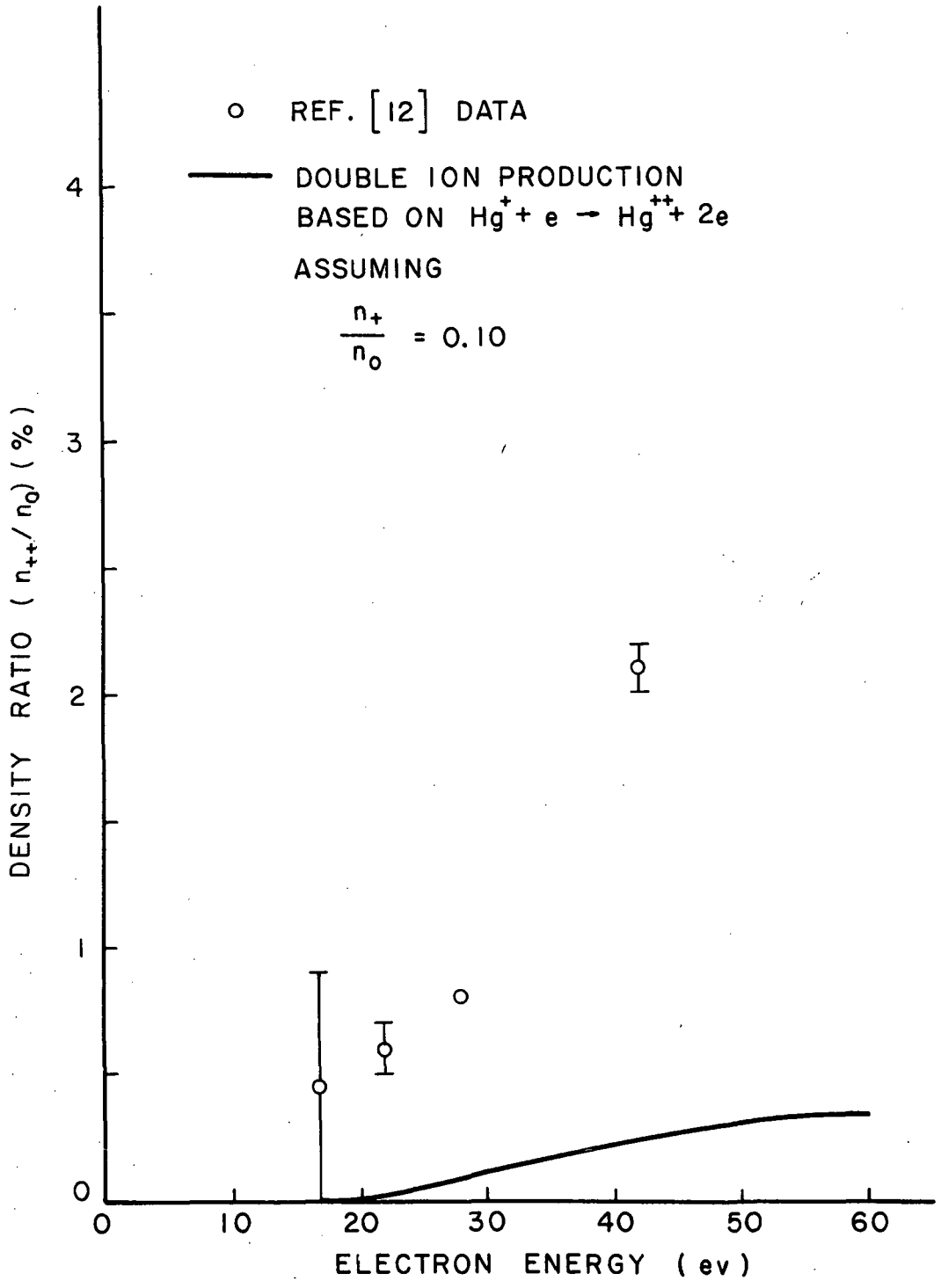

FIGURE 28. DOUBLE ION PRODUCTION FROM SINGLE IONS

3) Production of double ions by electrons in the maxwellian energy tail is significant.

4) The ionization potential assumed for the ten d electrons of the single ionic state is too high.

THERMAL FLOW METER

In the course of conducting experimental studies of mercury bombardment thrusters, considerable time is consumed in waiting to obtain accurate mercury flow rate information. This problem could be alleviated if a continuously indicating, accurate flow meter were available. The thermal flow meter measuring liquid flow rate has been proposed as a possible solution[4], and a small effort has been expended on the idea during the report period. The basic concept of this device is illustrated in Figure 29a. The reference thermistor and output thermistor are connected into a bridge circuit[4] so the bridge output is proportional to the temperature difference sensed by the two thermistors. This temperature difference is related to the flow rate since the rate of heat input is fixed. In order to analyze the flow meter the model of Figure 29b is considered. The flow is from left to right at velocity u. The heat is assumed to be supplied at a rate $\dot{q}$ ($\dot{q}_2$ to the upstream tube section and $\dot{q}_1$ to the downstream tube section) by a heater which has zero length and is located at position x = 0. The ends of the tube, located at ℓ_1 and $-\ell_2$, are held at an ambient temperature T_a.

The conduction equation which describes the temperature distribution in either section of the tube is:

$$\frac{u}{\alpha}\frac{dT}{dx} = \frac{d^2T}{dx^2} \tag{19}$$

where α is the thermal diffusivity of the fluid flowing in the tube. The solution to this equation is:

$$T = Be^{ux/\alpha} + C \tag{20}$$

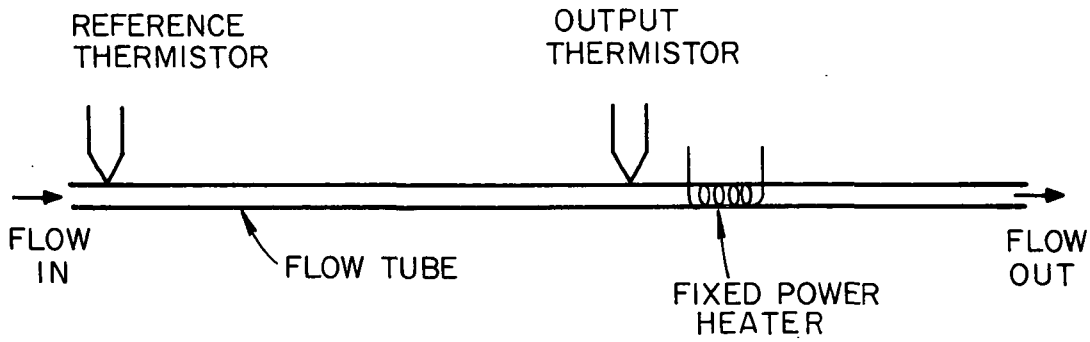

a) THERMAL FLOW METER SCHEMATIC

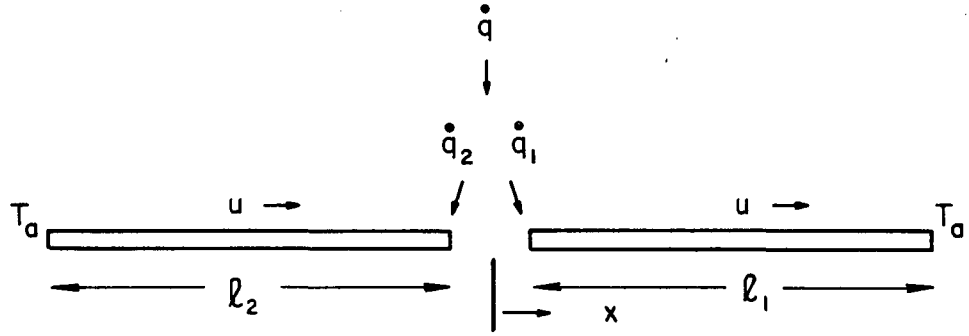

b) THERMAL FLOW METER ANALYTICAL MODEL

FIGURE 29. THERMAL FLOW METER

The boundary conditions for the two sections are:

upstream section	downstream section
$T = T_a$ @ $x = -\ell_2$	$T = T_a$ @ $x = \ell_1$
$T = T_o$ @ $x = 0$	$T = T_o$ @ $x = 0$

where T_o is the temperature at the heater. This temperature will be determined by the heat input rate $\dot{q}$ through a global energy balance on the tube.

Application of the boundary conditions to equation (20) yields the following solution:

$$\frac{T - T_a}{T_o - T_a} = 1 - \frac{e^{ux/\alpha} - 1}{e^{u\ell_1/\alpha} - 1} \quad , \quad \ell_1 \geq x \geq 0 \tag{21}$$

$$\frac{T - T_a}{T_o - T_a} = 1 - \frac{1 - e^{ux/\alpha}}{1 - e^{-u\ell_2/\alpha}} \quad , \quad -\ell_2 \leq x \leq 0 \tag{22}$$

Considering the sketch once again one sees:

$$\dot{q} = \dot{q}_1 + \dot{q}_2 \tag{23}$$

The heat supplied to the upstream section must either be convected out of the tube at $x = 0$ or conducted out at $x = -\ell_2$. Hence one has:

$$\dot{q}_2 = KA \left(\frac{dT}{dx}\right)_{x = -\ell_2} + \rho AuC\ (T_o - T_a) \tag{24}$$

where A is the cross sectional area of the tube, k, ρ, and C are respectively the conductivity, density and specific heat of the working fluid. Similarly for the downstream section of the tube one has

$$\dot{q}_1 = -\ KA \left(\frac{dT}{dx}\right)_{x = \ell_1} - \rho AuC\ (T_o - T_a) \tag{25}$$

Solving for the temperature gradients at ℓ_1 and $-\ell_2$ from equations (21) and (22), substituting these into equations (24) and (25) and combining with equation (23) one can determine the temperature at the heater T_o.

$$T_o = T_a + \frac{\dot{q}}{\rho A u C} \frac{1}{\left[\frac{e^{-u\ell_2/\alpha}}{1 - e^{-u\ell_2/\alpha}} + \frac{e^{u\ell_1/\alpha}}{e^{u\ell_1/\alpha} - 1}\right]} \tag{26}$$

Substituting equation (26) into equations (21) and (22) the following temperature profile expressions are obtained:

$$(T - T_a)\ \frac{\rho A u' C}{\dot{q}} = \left(\frac{u'}{u}\right) \frac{\left[1 - \frac{e^{ux/\alpha} - 1}{e^{u\ell_1/\alpha} - 1}\right]}{\left[\frac{e^{-u\ell_2/\alpha}}{1 - e^{-u\ell_2/\alpha}} + \frac{e^{u\ell_1/\alpha}}{e^{u\ell_1/\alpha} - 1}\right]} \qquad \ell_1 \geq x \geq 0 \tag{27}$$

where u' is the design flow velocity, i.e. one intermediate to the velocity range of interest.

$$(T - T_a)\ \frac{\rho A u' C}{\dot{q}} = \left(\frac{u'}{u}\right) \frac{\left[1 - \frac{1 - e^{ux/\alpha}}{1 - e^{-u\ell_2/\alpha}}\right]}{\left[\frac{e^{-u\ell_2/\alpha}}{1 - e^{-u\ell_2/\alpha}} + \frac{e^{u\ell_1/\alpha}}{e^{u\ell_1/\alpha} - 1}\right]} \qquad -\ell_2 \leq x \leq 0 \tag{28}$$

These equations are shown plotted in Figure 30a for a properly designed flow meter. The vertical axis is nondimensional temperature $\frac{(T-T_a)\rho A u' C}{\dot{q}}$ and the horizontal axis is nondimensional axial position $\frac{u'x}{\alpha}$. The parameter is nondimensional flow velocity which is examined here over the range 1/5 of design flow to 4 times design flow.

If the flow tube nondimensional lengths, $\frac{u'\ell_1}{\alpha}$ and $\frac{u'\ell_2}{\alpha}$ are insufficient the device will exhibit excessive conduction losses and the temperature difference will not be a strong function of flow rate, as illustrated in Figure 30b.

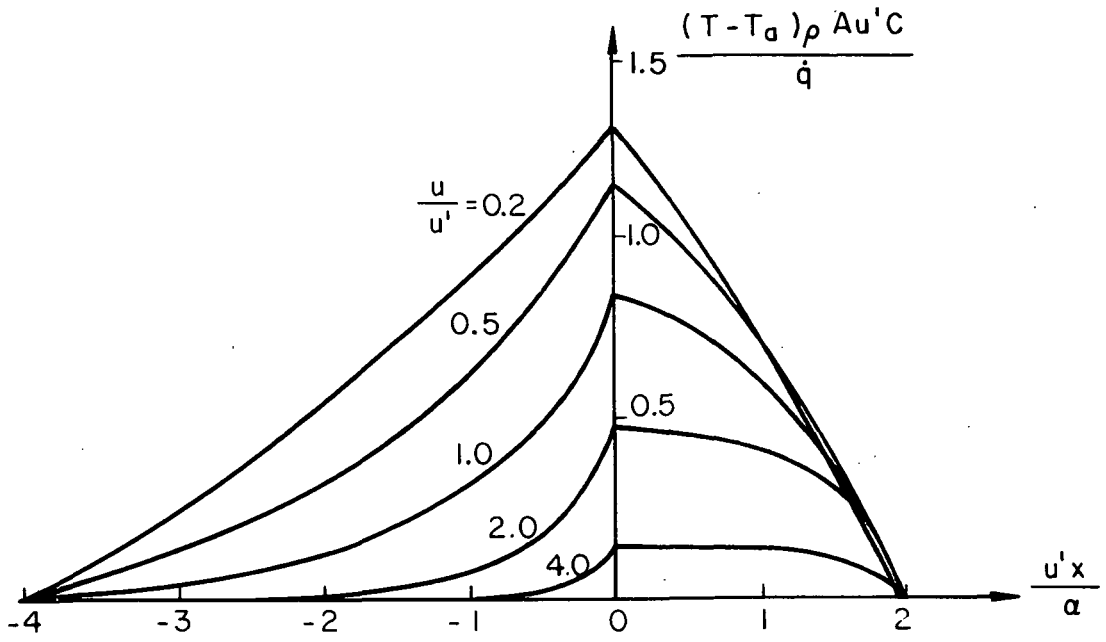

a) PROPERLY DESIGNED FLOW METER

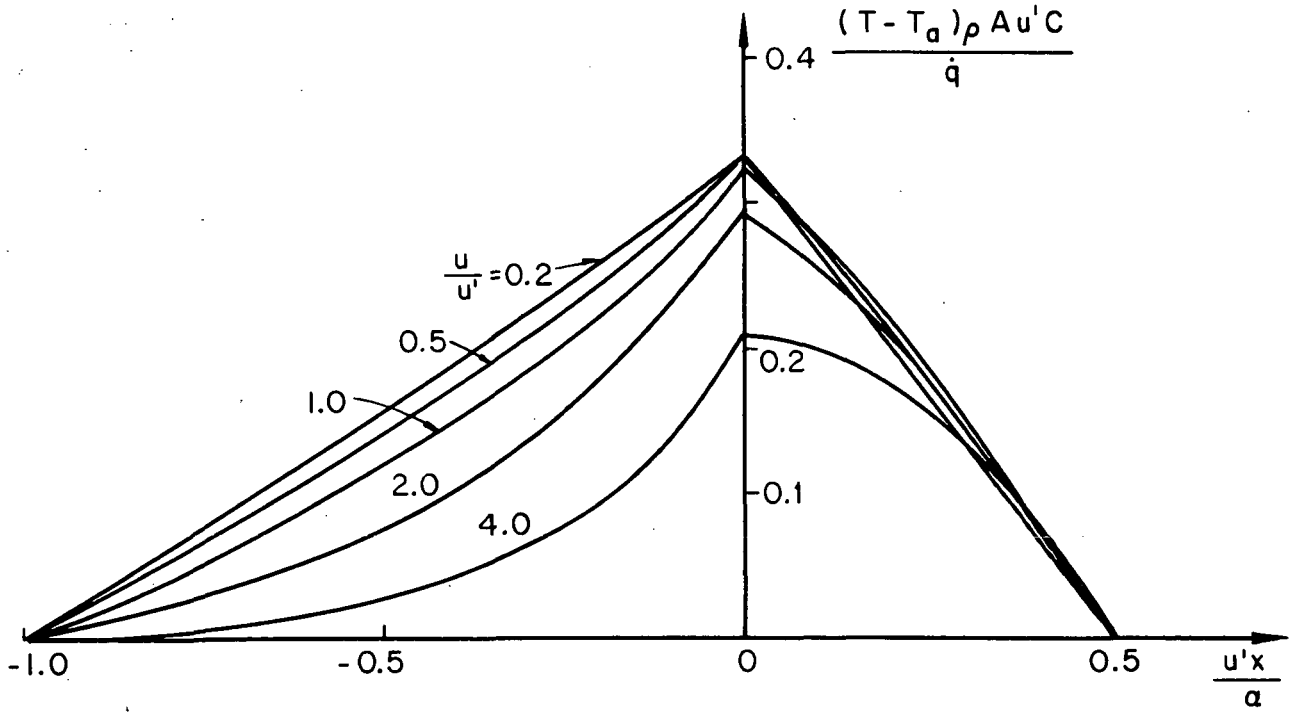

b) FLOW METER WITH EXCESSIVE CONDUCTION LOSSES

FIGURE 30. THEORETICAL THERMAL FLOW METER TEMPERATURE PROFILES

A flow meter has been built, using 0.30 mm inside diameter teflon tubing for the tube and a 26 milliwatt heater. The entire flow tube is enclosed in a vacuum chamber so spurious convective heat transfer from the system is minimized. The system was designed for a 100 ma eq midrange flow rate. It is designed to produce the temperature profiles of Figure 30a, having tubes lengths, ℓ_1 = 4.2 cm and ℓ_2 = 8.4 cm. Thermistors are located at $\frac{xu'}{\alpha} \approx -0.2$ and $\frac{xu'}{\alpha} \approx -3.8$ (Figure 30a).

The flow meter has been tested using a small variable speed, positive displacement pump to produce the desired flow rates. Typical flow rate input and flow meter bridge output obtained with this system are shown in Figure 31. The flow rate input shown in the upper portion of the figure is not exactly correct as the pump plunger tends to stick and then jump, producing a jagged flow pattern which is evident in the bridge output data. The flow meter is seen to have a time constant of the order of 6 minutes and a sensitivity of about 0.03 mv/ma eq.

Although this vacuum isolation of the flow tube has eliminated most of the noise associated with the flow meter, Figure 31a shows a 2% drift in the zero over the duration of the test shown. This drift has been observed on a number of tests, and it appears to be due to changes in ambient temperature of the incoming mercury (thermistor resistance is not a linear function of temperature in this temperature range).

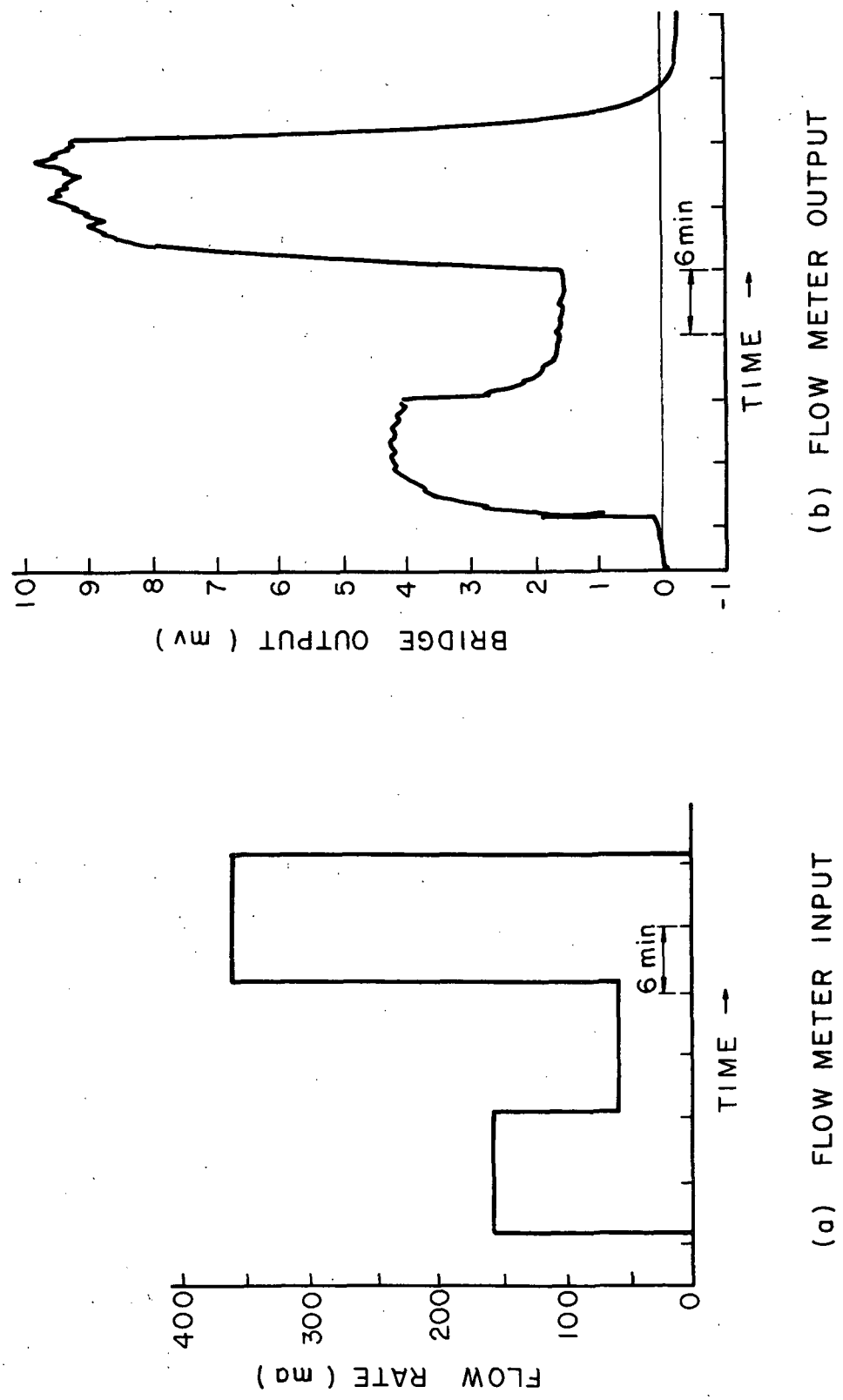

FIGURE 31. TYPICAL THERMAL FLOW METER OUTPUT

REFERENCES

1) Wilbur, P. J., "Effects of the Hollow Cathode Discharge on Throttled Ion Thruster Performance," AIAA Paper No. 72-421, April 17-19, 1972.

2) Byers, D.C. and Staggs, J. F., "SERT II Flight-Type Thruster System Performance," AIAA Paper No. 69-235, March 3-5, 1969.

3) Bechtel, R. T., et al., "Performance of a 15-centimeter Diameter, Hollow-Cathode Kaufman Thruster," AIAA Paper No. 68-88, January 22-24, 1968.

4) Wilbur, P. J., "An Experimental Investigation of a Hollow Cathode Discharge," CR-120847, December 1971, NASA.

5) Kerslake, W. R., et al., "Flight and Ground Performance of the SERT II Thruster," J. Spacecraft and Rockets, V. 8, No. 3, March 1971.

6) Knauer, W., et al., "Radial Field Kaufman Thruster," J. Spacecraft and Rockets, Vol. 7, No. 3, p. 249, March 1970.

7) King, H. J., et al., "2½ KW Low Specific Impulse, Hollow Cathode Mercury Thruster," AIAA Paper No. 69-30, March 3-5, 1969.

8) Kaufman, H. R., "Ion Thruster Propellant Utilization," Ph.D. Thesis, Colorado State University, June 1971.

9) Wells, A. A. "Current Flow Across a Plasma 'Double Layer' in a Hollow Cathode Ion Thruster," AIAA Paper No. 72-418, April 17-19, 1972.

10) Poeschel, R. L. and W. Knauer, "A Variable Magnetic Baffle for Hollow Cathode Thrusters," AIAA Paper No. 70-175, January 19-21, 1970.

11) Young, H. D., Statistical Treatment of Experimental Data, p. 126f. McGraw-Hill, 1962.

12) Milder, N. L. and J. S. Sovey, "Characteristics of the Optical Radiation from Kaufman Thrusters," NASA TN D-6567, November 1971.

13) Masek, T. D., "Plasma Properties and Performance of Mercury Ion Thrusters," AIAA Paper 69-256, March 1969.

14) Bleakney, W., "Probability and Critical Potentials for the Formation of Multiply Charged Ions in Mercury Vapor by Electron Impact," Phys. Rev. 35, pp 139-148, January 1930.

15) Pawlik, E. V., et al., "Ion Thruster Performance Calibration," AIAA Paper No. 72-475, AIAA 9th Electric Propulsion Conference, April 1972.

16) Gryzinski, Michal, "Classical Theory of Atomic Collisions. I. Theory of Inelastic Collisions," Phys. Rev. Vol. 138, No. 2A, p. A341, April 19, 1965.

17) Moore, C. E., "Atomic Energy Levels," Ntl. Bur. Std. (U.S.), Circ. No. 467 (1958).

Distribution List

	Number of Copies
National Aeronautics and Space Administration Washington, D.C. 20546	
Attn: RPE/James Lazar	1
Harold Kaufman	1
National Aeronautics and Space Administration Lewis Research Center 21000 Brookpark Road Cleveland, Ohio 44135	
Attn: Research Support Procurement Section	
W.E. Park, MS 500-312	1
Technology Utilization Office, MS 3-19	1
Management Services Division, MS 5-5	1
Library, MS 60-3	2
Spacecraft Technology Division, MS 54-1	
W. Plohr	1
E. Davison	1
R. Finke	1
D. Byers	1
B. Banks	1
P. Thollot	1
W. Kerslake	10
Electromagnetic Propulsion Division, MS 301-1	
W. E. Moeckel	1
G. Seikel	1
Report Control Office, MS 5-5	1
National Aeronautics and Space Administration Marshall Space Flight Center Huntsville, Alabama 35812	
Attn: Ernst Stuhlinger (M-RP-DIR)	1
C. H. Guttman	1
Research and Technology Division Wright-Patterson AFB, Ohio 45433	
Attn: (APIE-2) R. Johnson	1
National Aeronautics and Space Administration Scientific and Technical Information Facility P. O. Box 33 College Park, Maryland 20740	
Attention: NASA Representative RQT-2448	6

Case Institute of Technology
10900 Euclid Avenue
Cleveland, Ohio 44106
Attn: Mr. Eli Reshotko 1

Gruman Aircraft Engineering Corporation
Bethpage, Long Island, New York 11101
Attn: Mr. L. Rothenberg 1

Royal Aircraft Establishment
Space Department
Franborough, Hants, England
Attn: Dr. D. G. Fearn 1

United Kingdom Atomic Engergy Authority
Culham Laboratory
Abingdon, Berkshire, England
Attn: Dr. A. A. Wells 1
Dr. M. F. Harrison 1

National Aeronautics and Space Administration
Goddard Space Flight Center
Greenbelt, Maryland 20771
Attn: Mr. W. Isley, Code 734 1
Mr. R. Hunter 1

SAMSO (SYAX/Capt. D. Teal) 1
Air Force Unit Post Office
Los Angeles, California 90045

Comsat Laboratories
P. O. Box 115
Clarksburg, Maryland 20734
Attn: B. Free 1

Rocket Propulsion Laboratory
Edwards AFB, California 93523
Attn: LKDA/Lt. S. Rosen 1
Mr. Clark Hawk 1

DFVLR
33 Braunschweig
Bienroder Weg 53
West Germany
Attn: Dr. G. F. Au 1

Giessen University
1st Institute of Physics
Giessen, West Germany
Attn: Professor H. W. Loeb 1

Jet Propulsion Laboratory
4800 Oak Grove Drive
Pasadena, California 91102
Attn: D. Bartz 1
Technical Library 1
E. Pawlik 1
D. Fitzgerald 1

Electro-Optical Systems, Inc.
300 North Halstead
Pasadena, California 91107
Attn: Mr. R. C. Speiser 1
Mr. R. Worlock 1

TRW Inc.
TRW Systems
One Space Park
Redondo Beach, California 90278
Attn: Mr. E. Cohen 1
Dr. H. Meissinger 1
Dr. J. M. Sellen 1

Westinghouse Astronuclear Laboratories
Electric Propulsion Laboratory
Pittsburgh, Pennsylvania 15234 1

National Aeronautics and Space Administration
Ames Research Center
Moffett Field, California 94035
Attn: Dr. F. Casal 1

National Aeronautics and Space Administration
Langley Research Center
Langley Field Station
Hampton, Virginia 23365
Attn: Technical Library 1

Hughes Research Laboratories
3011 Malibu Canyon Road
Malibu, California 90265
Attn: Mr. J. H. Molitor 1
Dr. H. J. King 1
Dr. R. L. Poeschel 1
Mr. R. Vahrenkamp 1

United States Air Force
Office of Scientific Research
Washington, D.C. 20025
Attn: Mr. M. Slawsky 1

Air Force Academy, Colorado 80840
Attn: Major W. B. Adams 1

Princeton University
Princeton, New Jersey 08540
Attn: Dr. W. F. Von Jaskowsky 1
Dean R. G. Jahn 1
Dr. K. E. Clark 1

The City University
Department of Aeronautics
St. John Street
London ECIV 4PB, England
Attn: Antony Martin 1

Communications Research Centre
Ottawa, Ontario, Canada
Attn: W. F. Payne 1